Anul XXXIX 1994

STUDIA
UNIVERSITATIS BABEŞ-BOLYAI

PHYSICA

1

Editorial Office: 3400 CLUJ-NAPOCA str. M. Kogălniceanu nr 1 ▸ Telefon : 116101

SUMAR - CONTENTS - SOMMAIRE

STUDIA UNIV. BABEŞ-BOLYAI, PHYSICA, XXXIX, 1, 1994

THEORETICAL PREDICTIONS OF NON-LINEAR INFRARED SPECTRUM FOR SF_6 AT 30 K USING A SIMPLE MODEL

C. FALUB* and I. DEAC**

Received. 15.06.1994

ABSTRACT. - We presented a theoretical prediction of collisionless multiphoton absorbtion at low temperature in SF_6 and used to interpret the recent experimental results. A computationally simple model describes the excitation process on the first three vibrational levels of ν_3 mode for SF_6 molecules.

INTRODUCTION

During the last 15 years or so considerable efforts have been devoted to developing a comprehensive theory of infrared multiphoton absorbtion (IRMPA) and dissociation (IRMPD) in different types of polyatomic molecules Many of these works emphasized a spectroscopically accurate description of excitation through the infrared modes Among the heavy spherical top molecules SF_6 is probably the one which has received the most attention to the date These system molecular parameters derived from high-resolution spectroscopy [1] allowed quantitative calculations to be performed [2-6] and the comparison with experiments using gas dynamically cooled SF_6 [7] The refinement of such calculations and experiments,and their intercomparison,offer the posibility for gaining a full quantitative understanding of the initial stages of multiphoton absorbtion.

In present paper we have explored a simple computationally convenient model and we

* *"Babeş-Bolyai" University, Faculty of Physics, 3400 Cluj-Napoca, Romania*

** *Institute for Isotopic and Technology, 3400 Cluj-Napoca, P.O.Box. 700, Romania*

have studied the infrared nonlinear absorbtion spectra of SF_6 molecules vs. laser frequency taking into account the ro-vibrational structure of the lower discrete levels of the IR active ν_3 mode.It was assumed that the time averaged populations of the top most vibrational level of the ν_3 mode (taken to be $3\nu_3$ following the experimental results of Alimpiev *et al* [7]), established through the coherent excitation of ν_3 states determines the transition rate to the quasicontinuum.

THEORY

The basic theory describing the excitation of ν_3 mode vibration-rotation states by an intense infrared laser is developed elsewhere [2].The basic problem is to solve the time dependent Scrödinger equation:

$$(H-i\hbar\partial/\partial t)\psi=0 \tag{1}$$

in the rotating wave approximation.

The Hamiltonian H can be split into two parts:

$$H=H_0+V(t) \tag{2}$$

where H_0 is diagonal in the $|nJ\rangle$ basis.The eigenvectors are defined by:

$$H_0|nJ\rangle=E(n,J)|nJ\rangle \tag{3}$$

where n and J are the vibrational quantum and total angular momentum quantum numbers, respectively. The interaction V(t) between the molecule and the laser is written as:

$$V(t)=-\mu_0 E_0 \cos(\omega_0 t) \tag{4}$$

where E_0 is the classical electric field amplitude of the laser which is taken to be polarized along a spaced-fixed Z axis,μ_0 is the component of the molecular dipol moment along this

axis and ω is the angular frequency of the laser.

Using the effective Hamiltonian formalism [2] to solve multiphoton dynamics problem we have computed non-linear absorbtion spectrum of SF_6 using several approximating conditions:

-the energy is given by the expression:

$$E(n,J)=n\upsilon_3+n(n-1)\chi_{33}+(B_0-\alpha n)J(J+1) \tag{5}$$

where the spectroscopic constants have their usual meanings and their values are the same as those used by Hodgkinson *et al*[4]

-the non-diagonal elements of the effective Hamiltonian are supposed to be independent of J:

$$\langle nJ|\mu E|n+1,J\rangle=\sqrt{n+1}\ \mu_{01}E \tag{6}$$

where μ_{01} is the standard dipol matrix element for the fundamental transition,

-in relationship (5) the anharmonic splittings of the n>1 levels are neglecting;

-at low temperature (<100 K) the vibrational ground state $|0J\rangle$ is completely populated

The population distribution vs. different values of rotational number levels has been corected taking into acount the nuclear spin corrections

DESCRIPTION OF COMPUTER PROGRAMME

The effective Hamiltonian formalism to solve the time-dependent equation has been transposed in Turbo Pascal

The computing algorithm of multiphoton spectrum include several procedures:

-the sequence of numerical estimation for Maxwell-Boltzmann distribution on the ground vibrational state;

-the sequence of computing energies levels for ν_3 mode of SF_6 molecules,and non-diagonal elements of the effective Hamiltonian for a fixed value of laser intensity and the angular frequency of the laser radiation ;

The symmetric matrix of the effective Hamiltonian has been diagonalised by the Jacobi procedure.With the eigenvalues and eigenvectors obtained we computed the time averaged populations for SF_6 molecules excited on the first three vibrational levels. In order to obtain the IRMPA spectra,the above mentioned sequences was repeated for laser frequencies from 944 cm^{-1} to 949 cm^{-1}

RESULTS AND COMPARISON WITH EXPERIMENT

Alimpiev and coworkers [7] have measured multiphoton absorbtion spectra in SF_6 at 30 K by exciting gas-dynamically cooled SF_6 with two lasers.The initial excitation was provided by a high pressure CO_2 laser (fluence Φ_1=0.135 J/cm^2,pulse time 40 ns) which was tuned in ν_3 absorption band.Excited molecules were dissociated by a second higher-power laser (Φ_2=40 J/cm^2) which was considerable detuned from ν_3 fundamental band (ν=938.69 cm^{-1}). The observed signal was the luminiscence from HF^* formed from liberated fluorine atoms and hydrogen carrier gas to having only three major peaks which are centred on 944.39 cm^{-1},945.62 cm^{-1} and 947.97 cm^{-1} (Fig 1).

In the same figure also the numerically results obtained by Hodgkinson and Taylor [4] using an effective Hamiltonian which include the effects of first order Coriolis interaction and

the octahedral splits for the vibrational levels with n>1 are given They have estimated the average number of photons absorbed per molecule at 30 K and 10 MW/cm^2 laser intensity

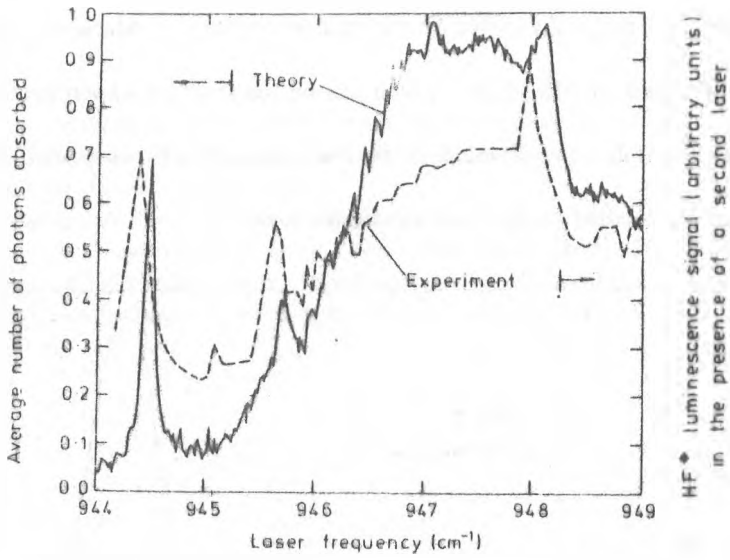

Fig.1 Experimental and theoretical multiphoton absorbtion spectra for SF_6 at 30 K The experimental spectrum (Alimpiev and coworkers [7]) was obtained by exciting the supercooled SF_6 molecules using two CO_2 laser pulses The HF^* luminescence is a measure of the dissociation probability The theoretical spectrum is a prediction of the average number of photons absorbed by SF_6 for a laser intensity of 10 MW/cm^2.

Our theoretical prediction of the time-averaged population at 30 K and 10 MW/cm^2 is shown in Fig 2.As it can be seen it has the same overall shape as the experimental spectra and also the three prominent resonant peaks centred on 944.40 cm^{-1}, 946 13 cm^{-1} and 947 86 cm^{-1} These corespond very well to the experimental and Hodgkinson prediction of resonace positions.

The three obtained resonance corespund to two-photon excitation of the A_{1g},E_g,and F_{2g} sublevels of the 2 ν_3 overtone state [4] These resonances can be obtained using the P(20), P(18) and P(16) laser lines for excitation,respectively

Althogh we used a simplified model in comparison with the Hodgkinson and Taylor model,the fit between the experimental data and the teoretically predicted values is better This is true especially for the peaks at 946.39 cm^{-1} and 947.97 cm^{-1}. Moreover, one can notice the presence of a peak at 945.31 cm^{-1} which can be found in the experimental spectrum at 945.11 cm^{-1}.Our simple model would allow the assigment of this peak,if the excitation mechanism can be detalied on the each vibrational level.

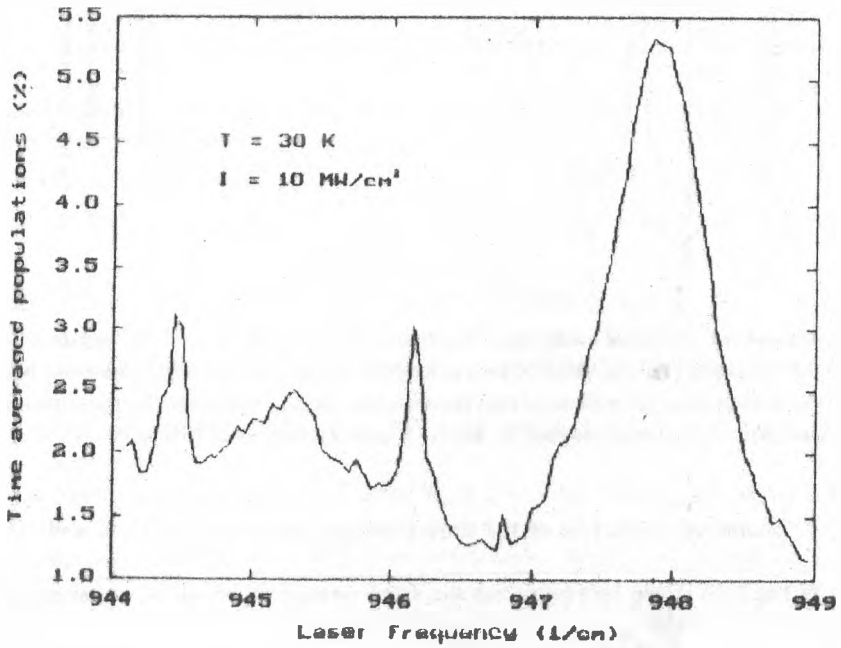

Fig.2 Our theoretical prediction for the time averaged population by SF_6 at 30 K and a laser intensity of 10 MW/cm^2

CONCLUSIONS

In conclusion,there is an excellent agreement between our theoretical predictions and experimental data on multiphoton absorbtion in super-cooled SF_6.This allows an improved

quantitative understanding of the initial stages of multiphoton excitation in SF_6 and similar molecules.

REFERENCES

1. Patterson,C.W.,Krohn,B.J.,and Pine,A.S.,*J.Molec.Spectrosc.*, **80**,133,1981.
2. D.M.Larsen,N.Bloembergen,*Opt.Commun.*,**17**,254,1976
3. D.M.Larsen,*Opt.commun.*,**19**,404,1976.
4. D.P.Hodgkinson,A.J.Taylor,*Mol.Physics*,**52**,1017,1984.
5. V.Tosa,I.Deac,P.Mercea,Z.S.Gulacsi and V.Mercea,*Appl.Phys.*,**B 36**,55,1984.
6. S.S.Mitra and S.S.Bhattacharyya,*J.Phys.*,**B.At.Mol.Opt.Phys.**, **25**,2535,1992.
7. S.S.Alimpiev,N.N.Karlov,S.M.Nikiforov,B.G.Sartakov and A.L. Shtarkov,*Laser Conference*,New Orleans,1981.

STUDIA UNIV. BABEŞ-BOLYAI, PHYSICA, XXXIX, 1, 1994

IR STUDY OF THE COORDINATION MODE OF Cu(II) ION IN METHAZOLAMIDE COMPOUND

I.DAVID*, V.CHIŞ*, O.COZAR*, R.SEMENIUC**, S.NEGURICI*

Received: 13.02.1994

ABSTRACT. - The assignment of the main absorption bands from the IR spectra of methazolamide and its copper(II) complex was achieved. The shifts of some bands and the appearance of the other new bands in the spectrum of the metal complex are explained by the participation of water, pyridine and methazolamide molecules to the coordination.

1. Introduction. It is known that sulphonamide causes an inhibition of the zinc metalloenzyme carbonic anhydrase [1]. The metal complexes having analogous methazolamide {[N(4-methyl-2-sulphamoxyl-Δ-1,3,4-thiadiazolin-5-ylidine)],acetamide} (Hmacm) as ligand were studied because in these substituted the N(thiadiazole) atom closest to the acetamide groups probably hampers the coordination via the nitrogen atoms of the ring, a similar way to that observed in the active site of metalloenzyme [2].

The $Cu(macm)_2(py)_2(H_2O)_2$ complex was prepared as previously reported [3] and its structure determined by X-ray diffraction [3] is given in Fig.1. This provides a new example of the energetic preference of the elongated coordination in Jahn-Teller distorted octahedral copper complexes [4]. The structure consists of centrosymmetric complex units in which the metallic ion, occupies the centre symmetry in an octahedral site with two pyridine nitrogen atoms [N(15) and N(15)*] and two sulphonamidato nitrogen [N(8) and N(8)*] of the

* *"Babeş-Bolyai" University, Faculty of Physics, 3400 Cluj-Napoca, Romania*

** *"Babeş-Bolyai" University, Faculty of Chemistry, 3400 Cluj-Napoca, Romania*

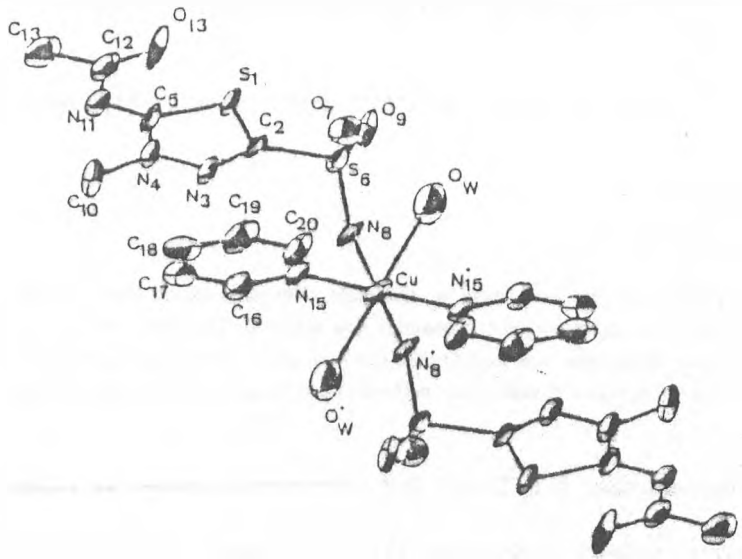

Fig.1 The structure of the $Cu(macm)_2(py)_2(H_2O)_2$ complex.

methazolamidato anions, coordinated in the equatorial plane. Two oxygen atoms from two water molecules are placed in the axial positions (*Oz*).

IR absorption spectra were recorded in KBr pellet form on a Perkin-Elmer 843 spectrophotometer.

2. Results and discussion. The IR spectrum of methazolamide is shown in Fig.2a.

The bands which appear at 3240cm^{-1} and 3192cm^{-1} may be assigned to the ν_{as}(N-H) vibration of the sulphonamide group, and the 3041cm^{-1} band to the ν_s(N-H) vibration of the same group.

The IR spectrum presents a strong band at 1600cm^{-1} attributed to ν(C=O) vibration of the acetamide group [5].

The strong band which appears at 1480cm^{-1}, together with another two lower bands at 1458cm^{-1} and 1440cm^{-1} are attributed to a combination of ν(C=N) vibration of the thiazole ring with the δ(N-H) deformation vibration of the sulphonamide group. The 1380cm^{-1} and 1360cm^{-1} bands are due to the $\delta_{as}(CH_3)$ deforming vibrations from acetamide group and thiadiazol ring [6].

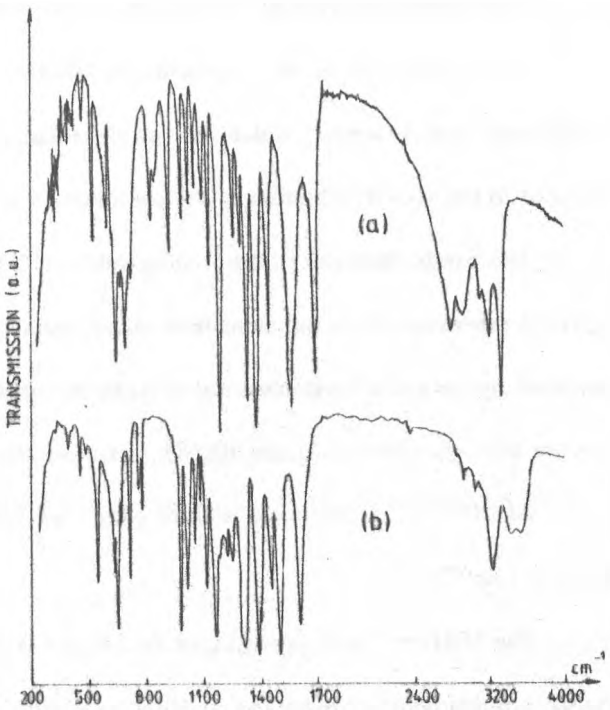

Fig.1 IR spectra of the methazolamide (a) and $Cu(macm)_2(py)_2(H_2O)_2$ complex (b).

At 1309cm^{-1} and 1174cm^{-1} the IR spectrum presents two strong bands which are typical for $\nu_{as}(SO_2)$ and $\nu_s(SO_2)$ vibrations.

The middle intensity band from 1000cm^{-1} can be attributed to the ν(N-N) vibration.

The band at 933cm^{-1} may be assigned to the ν(S-N) vibration.

At 750cm^{-1} there is a band which is attributed to the $\gamma(CH_3)$ vibration of the thiadiazol ring.

At 700cm^{-1} there is a weak band which corresponds to the δ(N-H) vibration besides the plane of the sulphonamide group.

The bands at 637cm^{-1} and 609cm^{-1} are due to a combination of the ν(C-S) vibration

of the thiazole ring and the sulphonamide group

The doublet observed at 530-510cm^{-1} is attributed to the vibration of SO_2 group

The IR spectrum of the $Cu(macm)_2(Py)_2(H_2O)_2$ complex (Fig 2b) presents two bands at 3550cm^{-1} and 3450cm^{-1}, which are not observed in the free methazolamide spectrum, assigned to the ν(O-H) vibration of the coordination water molecules

The bands observed in the free ligand at 3240cm^{-1} and 3192cm^{-1} assigned to the ν_{as}(N-H) vibration of the sulphonamide group are replaced in the copper(II) complex IR spectrum by only one band observed at 3230cm^{-1}. This fact may be explained taking into account the deprotonation of the SO_2NH^- group interacting with metal ion

At 3057cm^{-1} is observed a little band due to the characteristic vibrations of the pyridine ring [7].

The 3041cm^{-1} band which in the free ligand is attributed to the ν_s(N-H) vibration of the sulphonamide group is not observed in the spectrum of the complex suggesting the loss of a proton of the SO_2NH_2 group

The band corresponding to the ν(C=O) vibration of the carbonyl of the acetamide group appears at the same frequency as in the methazolamide spectrum (1600cm^{-1})

At 1450cm^{-1} in the spectrum of the complex appears a new band of a medium intensity which is assigned to the characteristic vibration of the pyridine ring [8]

The bands from the 1380cm^{-1} and 1360cm^{-1} attributed for methazolamide to the $\delta(CH_3)$ vibration of the acetamide group are not modified, in agreement whit the data obtained from the RX diffraction studies

The $\nu_{as}(SO_2)$ vibration which in the spectrum of the ligand appears as a strong and

sharp band at 1309cm^{-1}, is present in the complex as a doublet at 1310-1280cm^{-1}

The band assigned to the $\nu_s(SO_2)$ vibration is shifted into the smaller frequencies (1150cm^{-1}) than those observed in the free ligand.

Two bands characteristic to the pyridine molecules coordinated at copper(II) ion appear at 1214cm^{-1} and 1080cm^{-1} [9]

The band assigned to the ν(N-N) vibration of a thiadiazol ring is not modified in the spectrum of the complex because the length of the N-N bond is not modified by coordination

At 970cm^{-1} is observed a strong and sharp band attributed to the ν(S-N) vibration, shifted with 40cm^{-1} relative to the same band of the free ligand

The doublet observed for the Cu(II) complex at 760-750cm^{-1} is assigned to the $\gamma(CH_3)$ and $\rho(H_2O)$ vibrations [10]

A new band assigned to the deformation vibration of the pyridine ring appears at 660cm^{-1}. It is shifted at higher frequencies indicating the presence of interaction between pyridine and metal ion

The doublet from 530-510cm^{-1}, which in methazolamide corresponds to the deformation vibration of the SO_2 group appears here (Fig 2b) as a single band at 530cm^{-1}.

The spectrum of the complex shows also a band at 440cm^{-1} which not appears in the spectrum of the ligand. This is characteristic for the deformation vibration of the pyridine ring outside of the plane [11].

As a trial, the bands from 470, 380 and 280^{-1} may be assigned to Cu-N (sulphonamide), Cu-OH and Cu-N (pyridine) vibrations respectively [12]

3. Conclusions IR spectra of the methazolamide and its Cu(II) complex allowed us to establish the vibrations whose frequencies are modified by coordination and also the new stretching vibrations in which the copper ion is involved

One of the N-H stretching vibrations of the NH_2 sulphonamide group present in the spectrum of the free ligand has disappeared in the spectrum of the metal complex due to the

deprotonation by the coordination of the nitrogen atom

The carbonyl ν(C=O) band is not changed comparatively with that of the methazolamide indicating the absence of the interaction between the acetamide group and the metal ions

The most significant modifications in the IR spectrum of the complex are the splitting and shifting to lower frequencies of the $\nu_s(SO_2)$ and $\nu_{as}(SO_2)$ bands. The change to higher frequencies of the ν(S-N) vibration is consistent with the coordination through the sulphonamide nitrogen atom.

The characteristic absorption bands of the coordinated pyridine molecules appear at 3057, 1450, 1215, 1080, 660 and 440cm^{-1}. These results confirm the presence of $CuN_2N_2^*O_2$ chromophore in agreement with X-ray data

REFERENCES

1. I Bertini, C.Luchinat, R.Monnanni, J Chem Educ., 62,924(1985)
2. S.Ferrer, J.G Haasnoot, R.A.G de Graff, J Reedijk, J.Borràs, Inorg.Chim Acta, 192,129(1992)
3. G.Alzuet, S.Ferrer, J.Borràs, A.Castineiras, X.Solans, M.Font-Bardia, Polyedron, 22,2849(1992)
4. E Bouwman, C E Westeide, W L.Driessen, J Reedijk, Inorg.Chim.Acta, 166,291(1989)
5. R.W Young, K H Wood, J.A.Eichler, J.R Vaughan Jr , J.Am.Chem.Soc , 78,4669(1956)
6. M Goldstein, M.A Russell, H.A Willis, Spectrochim. Acta, 25A,1275(1969)
7. E.Colacio, J.P.Costes, R.Kivekas, J.P.Laurent, J Ruiz, M.Sundberg, Inorg Chem , 30,1475(1991)
8. D.P Madden, M Nelson, J.Chem Soc A, 2342(1968)
9. N.S.Gill, R.M.Nuttall, D.E Scolte, D.W.A Sharp, J.Inorg Nucl Chem., 18,79(1961)
10. K.Nakamoto, Infrared spectra of inorganic and coordination compounds, John Wiley and Sons, New York, 1963
11. J.Robin, H.Clark, C.S.Williams, Inorg Chem , 4,350(1965)
12. B Prabhakar, P Lingaiah, K L. Reddy, Polyhedron, 9,805(1990)

STUDIA UNIV. BABEŞ-BOLYAI, PHYSICA, XXXIX, 1, 1994

ESR STUDY OF FREE RADICALS OBTAINED IN SOME GAMMA-IRRADIATED AMINOACIDS

V.CHIŞ*, O.COZAR*, G.DAMIAN*, L.DAVID*, C.COSMA*, R.SEMENIUC**, T.DRĂGOIU*

Received: 13.02.1994

ABSTRACT. - The ESR spectra of four powdered α-aminoacids (Glycine, L-Glutamic Acid, DL-Serine and DL-Asparagine) gamma irradiated at room temperature are examinated. The samples were irradiated with radiation doses ranging from 1.5KGy to 16.5KGy.

The dependence of the concentration of the free radicals with the irradiation dose is almost linear for DL-Serine and L-Glutamic Acid while it becomes constant for Glycine and DL-Asparagine in the range of 8-10KGy. In the case of DL-Serine and DL-Asparagine the ESR spectra were recorded for two levels of the microwave power, in order to identify the type of the dominant free radical which appears in these samples.

The carbon centred free radicals appear in these samples as a result of the deamination or by the hydrogen abstraction.

Introduction. Some of the most important results of the ESR spectroscopy have been obtained from the analysis of the hyperfine splitting in the spectra of the free radicals

The free radicals produced in irradiated aminoacids have been studied extensively [1]. Although the most precise ESR informations about radicals in solids are obtained from measurements on single crystals, however such measurements are possible for only a limited number of substances. The information which can be obtained from the ESR spectra of the free radicals in solids depends on the nature of the g and nuclear coupling (A) tensors

Generally, the free radicals are not kinetically stable entities. It is usual to associate stability with the delocalisation afforded by an extensive conjugated system. Indeed, many of

* *"Babeş-Bolyai" University, Faculty of Physics, 3400 Cluj-Napoca, Romania*

** *"Babeş-Bolyai" University, Faculty of Chemistry, 3400 Cluj-Napoca, Romania*

the studied free radicals have been π radicals in which the singly occupied orbital has π-symmetry [2]. The g values for all free radicals are close to that for the free electron indicating a weak spin-orbit coupling.

In order to obtain further information about the gamma radiation induced free radicals in biomolecules four different α-aminoacids (Glycine, L-Glutamic Acid, DL-Serine and DL-Asparagine) have been irradiated and investigated by ESR spectroscopy at room temperature.

Hyperfine couplings provides the key to identify the occurred free radicals, which usually appear as a result of the breaking of a C-N bond being removed an amino group or by loss of a hydrogen atom, leading to the carbon centred radicals [3,4].

Experimental. The powdered aminoacids investigated were purchased from FLUKA (DL-Asparagine), CHEMAPOL (DL-Serine) and SIGMA (Glycine and L-Glutamic Acid) and used without further purification. They were irradiated at room temperature, using a ^{60}Co gamma source of 31Gy/hour, with radiation dose ranging from 1.5KGy to 16.5KGy.

ESR measurements were performed at room temperature with a JEOL JES 3B spectrometer operating at 9.5GHz and with a ESP 300 E BRUKER spectrometer operating at 9.65GHz.

Results and discussion. The effect of the dose on the radical yield is shown in Fig.1 in which is plotted the maximum height of the ESR signal per 1mg of sample. The lines are guide for eye.

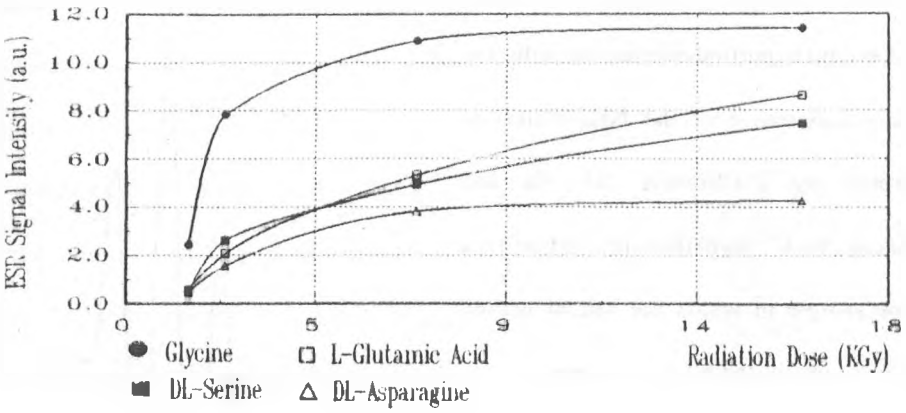

Fig.1 ESR signal intensity versus irradiation dose

As shown in this figure the number of the generated free radicals increases rapidly in the dose range up to 4KGy for all the irradiated aminoacids (especially for Glycine). The curves for DL-Serine and L-Glutamic Acid present an almost linear dependence in the whole range of the irradiation dose while for Glycine and DL-Asparagine they present a saturation in the range of 8-10KGy. These last curves can be explained taking into account the fact that by increasing the concentration of the free radicals the distance between them decreases and the radical-radical reactions compete with radical yielding [5] and so the concentration of the free radicals remains constant.

Glycine. The spectrum of the irradiated powdered glycine is shown in Fig.2 and consists of a triplet with a hyperfine splitting of 21G. The linewidth of the components is of about 9G and their intensity ratios is 1:2:1. This spectrum is assigned to the CH_2COO^- radical which is obtained by breaking of the C-N bond in neutral molecule of the glycine.

The hypothesis of the existence of the other radicals such as $CH_2^-NH_3$ or NH_2 is not

entertained. In the case of $CH_2'NH_2$ radical it would exhibit hyperfine interactions with five protons. Inexistence of the NH_2 radical is confirmed by J.R.Morton [6]. He has evidenced the C^{13} hyperfine interaction in a glycine sample in which the central carbon atom was substituted by C^{13} isotope.

The three lines of the spectrum are accompanied by two satellite lines having the overall spread of about 80G, being separated by main lines by an interval of 37G. These outer satellite lines which appear especially at high irradiation dose are assigned to a second radical $^{\cdot}NH_2CH_2COO^-$ [7].

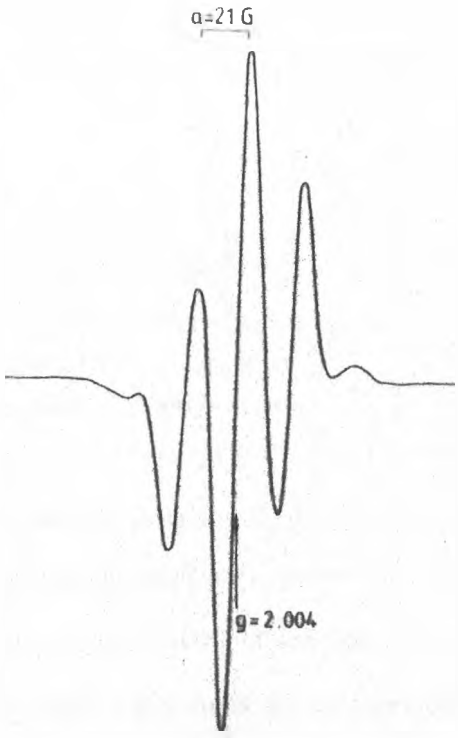

Fig.2 ESR spectrum of the gamma irradiated glycine (1.5KGy).

L-Glutamic Acid. Figure 3 shows the ESR spectrum of DL-Glutamic Acid which consists of six lines, a triplet with each component subsequently splitted in two components, attributed to the interaction of the unpaired electron on the α carbon with the α-proton (a_α=28G) and two β magnetically unequivalent protons ($a_{\beta 1}$=51G and $a_{\beta 2}$=10G). The α-proton coupling is close to that of the larger β-proton coupling likewise with X-irradiated L-α-Amino-n-butyric Acid Hydrochloride [8].

The obtained spectrum is assigned to the $COOCHCH_2CH_2COO^-$ radical.

DL-Serine. The spectrum of the irradiated DL-Serine is given in Fig.4 and it was

plotted for two power level in order to establish the radicals which are present in the sample

The spectrum for a power level of 2.78μW (Fig.4.a) exhibits a doublet due to an α-proton (a_{α}=60G), each component being splitted in four components arising from the interaction of the odd electron with two unequal coupled β-protons ($a_{\beta 1}$=22G, $a_{\beta 2}$=12G)

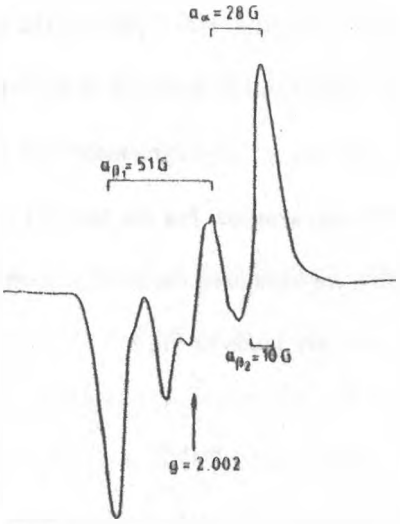

Fig.3 ESR spectrum of the gamma irradiated DL-Glutamic Acid (1.5KGy).

The proposed radical is $HOCH_2\dot{C}HCOO^-$.

By increasing of the power level one of the two paramagnetic species is saturated and

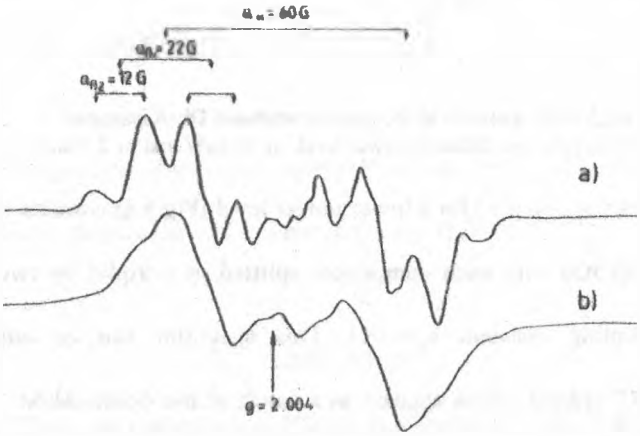

Fig.4 ESR spectrum of the gamma irradiated DL-Serine (1.5KGy) for two different power level: a) 2.78μW and b) 27.8mW

the obtained spectrum (Fig.4.b) consists only of a doublet due to the interaction of the

paramagnetic electron with a proton. The radical responsible for this spectrum and thus the dominant radical in DL-Serine is $HOCHC(^{+}NH_3)HCOO^{-}$.

These results are in good agreement with the others previously reported [9,10].

DL-Asparagine. For the analysis of the ESR spectrum of the gamma irradiated DL-Asparagine we have used the same procedure as for DL-Serine. The obtained spectra for two power levels are given in Fig.5.

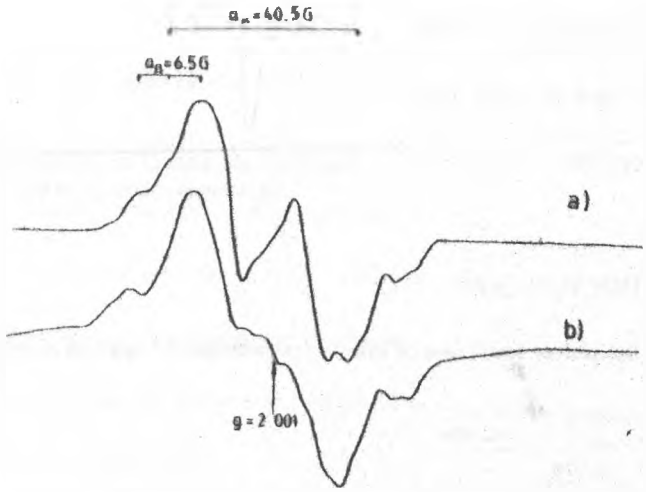

Fig.5 ESR spectrum of the gamma irradiated DL-Asparagine (1.5KGy) for two different power level: a) 8.63μW and b) 2.73mW.

The ESR spectrum obtained for a lower power level (Fig.5.a) consists of a doublet due to an α-proton (a_α=40.5G) with each component splitted in a triplet by two equivalent β-protons with a coupling constant a_β=6.5G. This spectrum can be attributed to the $(NH_2)COCH_2CHCOO^{-}$ radical which appears as a result of the deamination.

Figure 5.b shows the ESR spectrum of DL-Asparagine for a power level of 2.73mW which consists of a doublet due to an α-proton with a_α=40.5G, each component being subsequently splitted in two components by a β-proton with a_β=15G. This spectrum is

attributed to the $(NH_2)COCHCH(^{+}NH_3)COO^{-}$ radical which results from hydrogen abstraction, not from deamination. A similar conclusion is supported by Close et al. [11] from ESR and ENDOR investigation of the L-Asparagine·H_2O and L-Asparagine·D_2O.

Conclusions. The number of the free radicals generated by gamma irradiation in the investigated aminoacids increases rapidly with the irradiation dose up to 4KGy.

The ESR signal intensity of the Glycine and DL-Asparagine radicals shows a saturation in the range of 8-10KGy while the signal characteristic of the DL-Serine and L-Glutamic Acid radicals exhibits an almost linear dependence even for large values of the irradiation dose.

The occurred free radicals are the result of the breaking of a C-N bond or of the loosing of a hydrogen atom, leading to the carbon centred radicals in all the investigated samples. The hyperfine structure of the obtained spectra is due to the interaction of the paramagnetic electron with hydrogen or nitrogen nuclei.

Acknowledgments: We wish to thank Professor Marina Brustolon from University of Padova for useful discussion and the experimental facilities.

REFERENCES

1. W.Gordy "Theory and Applications of Electron Spin Resonance", John Wiley & Sons, 1980.
2. N.M.Atherton "Electron Spin Resonance-Theory and Applications", John Wiley & Sons, 1973.
3. H.Shields, Y.Haven, P.J.Hamrick Jr,, Y.Ma, Rad.Res., 116,373(1988).
4. N.A.Salih, O.Awadelkarim, A.Lund, Acta Chemica Scandinavica, 46,1140(1992).
5. Y.Lion, G.Denis, M.M.Mossetta, P.Riesz, Int.J Radiat.Biol., 43,71(1983).
6. J.R.Morton, J.Am.Chem.Soc., 86,2325(1964).

7. K.Nunome, H.Muto, K.Toriyama, M.Iwasaki, J.Chem.Phys., 65,3805(1976)
8. M.D.Shattuck, Y.Ma, M.Itoh, H.Shields, Rad.Res., 120,430(1989).
9. B.W.Castelman, G.C.Moulton, J.Chem.Phys., 57,2762(1972).
10. H.Shields, P.J.Hamrick Jr., J.Chem.Phys., 64,263(1975).
11. D.M.Close, G.W.Fouse, W.A.Bernhard, J.Chem.Phys., 4,1534(1977).

STUDIA UNIV. BABEŞ-BOLYAI, PHYSICA, XXXIX, 1, 1994

SURFACE-ENHANCED RAMAN SCATTERING OF 9, (10H) ACRIDONE ON SILVER SOLS

S. CÂNTĂ*, T. ILIESCU and S. CRĂCIUN**

Received: 10.05.1994

ABSTRACT. - Surface Enhanced Raman Scattering (SERS) of 9, (10H) Acridone [9,(10H)A] was studied in different types of colloids with different values of the surface potential. Ordinary Raman spectrum of solid [9,(10H)A] was obtained and compared to SERS spectra. The orientation of the [9,(10H)A] molecule and the posibility of bonding on the silver surface were established.

1. Introduction. Surface-Enhanced Raman Scattering (SERS) is used to be a very high sensitive technique in order to get informations about the nature of molecular adsorbate and the adsorbate-metal interaction mechanism. The electromagnetic and the chemical theories can explain the mechanism of the enhancement [1,2].

As an active surfaces are preferred colloidal silver hydrosols which present some advantages over silver electrodes. Silver sols are easely to prepare and the potential of the silver surface can be varied by changing the molar ratio of the sol's components [3].

In this paper we present our preliminary studies of SERS of [9,(10H)A]. The dependence of the enhancement mechanism on the surface potential and the orientation of the adsorbate on the silver surface were investigated.

* *"C.U.G." High School, Phys. Dept., B-dul Muncii 99-101, 3400 Cluj-Napoca, Romania*

** *"Babeş-Bolyai" University, Faculty of Physics, 3400 Cluj-Napoca, Romania*

2. Experimental. Silver colloids have been obtained by reduction of $AgNO_3$ with $NaBH_4$.

Three types of Ag colloids denoted as C_1, C_2 and C_3 with different values of the $NaBH_4$:$AgNO_3$ molar ratio have been prepared, according to the classic procedure [4].

$NaBH_4$ aqueous solution was cooled at ice-water temperature. $AgNO_3$ solution was added dropwise upon strong stirring.

The amount used for the mentioned types of colloids are given in Table 1.

The resulting colloids were bright yellow in different tintes with the λ_{max} of visible absorption spectra arround 400 nm. Fig. 1 presents the absorption spectrum of freshly prepared silver sol and after addition of [9,(10H)A] and $BaCl_2$ solution. The $BaCl_2$ was added in order to obtain the agregation of the sol which is a condition to obtain SERS spectra [1].

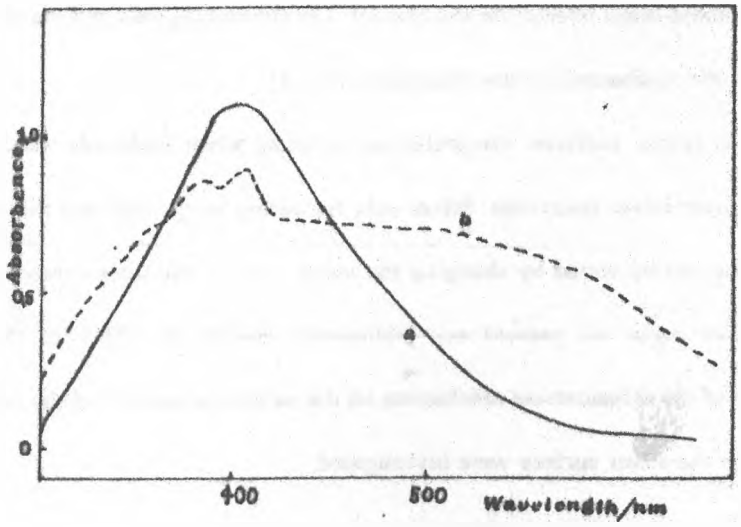

Fig. 1. Visible absorption spectrum of aqueous silver colloid C_1 (0.5cm cell pathlength): a) freshly prepared, b) after adition of acridone-ethanol solution and $BaCl_2$.

Table 1. The amounts used for preparing the silver sols.

Ag colloid	$NaBH_4$			$AgNO_3$			Molar ratio
	m (mg)	V (ml)	$c*10^3$ (mol/l)	m (mg)	V (ml)	$c*10^3$ (mol/l)	$NaBH_4$:$AgNO_3$
C_1	3.9	50	2.06	4.5	15	1.76	3.89
C_2	3.78	50	2	2.5	15	1	6.8
C_3	3.5	50	1.85	9	15	3.5	1.74

Triply distilled water was used to prepare the sols.

[9,(10H)A], with structural formula presented in Fig. 2, is a fluorescence compound. In order to eliminate this disadvantage for Raman investigation [9,(10H)A] was boiled with active coal to decreases the fluorescence. Purified p.a. ethanol was used to prepare the [9,(10H)A] solution.

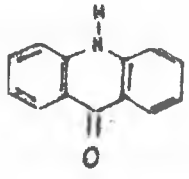

Fig. 2. Structural formula of 9, (10H) Acridone.

A small amount (20μl) of $1.5*10^{-3}$ mol/l [9,(10H)A] in ethanol was mixed with 1 ml silver sol C_1, then 10 μl, $2.3*10^{-2}$ mol/l $BaCl_2$ solution was added to obtain the final [9,(10H)A] concentration of $2.9*10^{-5}$ mol/l.

Addition of $BaCl_2$ solution drives to a colour change to mov. At the experiment time the colloids were aged for about 5 weeks. The Raman spectra were recorded on a GDM-1000

double monochromator using excitation with 488 nm radiation from an argon-ion laser. The spectral slit-width and the laser power are indicated in the figure legends. The scattered light from the sample placed in a 3mm glass tube, was collected at 90° geometry. All spectra were obtained at room temperature and within 5 min. after adding the [9,(10H)A] and $BaCl_2$ solution.

3. Results and Discussion. The ordinary Raman spectrum (ORS) of [9,(10H)A] in the solid state and the SERS spectra are presented in Fig. 3. as follows:

a) in silver sol C_1 without $BaCl_2$; b) in silver sol C_1 with $BaCl_2$; c) in silver sol C_2 with $BaCl_2$; d) in silver sol C_3 with $BaCl_2$

Changing the $NaBH_4$ to $AgNO_3$ molar ratio, in the preparation protocol of Ag colloid we have got a control over the potential of the Ag surface.

According to Čermáková et al. [3], the concentration of BH_4^- anion in the system decreases with the age of the colloid and this is equivalent with more positive potential of the Ag surface.

Admitting that the hydrolytic processes are the same in all of colloids, the most negative is C_2 and the most positive is C_3.

No one of C_1, C_2 and C_3 colloids one day aged did not give good SERS spectra. Two-three weeks aged colloids in dark storage, relates that the concentration of BH_4^- can be directly tuned toward more positive and stable potential of Ag surface and permit to obtain good SERS spectra.

The adsorption of [9,(10H)A] is promoted by a mean of our value of colloid potential

At a more positive value of the surface potential, the enhancement mechanism is reduced (Fig. 3d).

At a more negative potential (Fig. 3c) the bands of SERS spectrum are larger then that presented in Fig. 3b. The spectral data given in Table 2, a, b and c columns are correspond to a, b and c SERS spectra, respectively (Fig. 3).

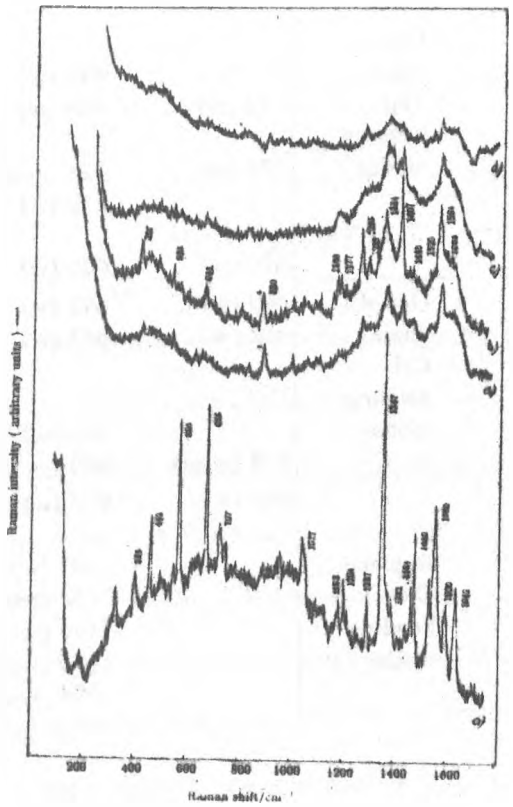

Fig. 3. Ordinary Raman spectrum (a) and SERS spectra of 6,(10H) acridone (a,b,c,d). Excitation with 488 nm (140 mW). Spectral slit-width 4 cm^{-1}. Asterisks indicate the ethanol band.

Table 2. Raman vibrational data for 9, (10H) Acridone (relative intensities in bracket). Spectral data for solid Acridine are given for comparison.

ORS*			SERS		
Solid [9,(10H)A]	Solid Acridine		a	b	c
	240			252 (w)	272 (w)
314 (w-m)**				292 (w)	307 (w)
386 (m)			392 (w)	396 (m)	392 (w)
	400				
	416				
		Out-of			
442 (s)		plane		440 (w)	436 (w)
	474	ring	472 (w)	468 (w)	477 (w)
	517	bending			
532 (w-m)		modes	528 (w)	528 (w-m)	532 (w)
550 (vs)	580			552 (w)	554 (w)
	613				
			620 (w)	620 (w)	612 (w)
		Out-of	642 (w)	642 (w)	
656 (vs)		plane	652 (w)	652 (w)	652 (w)
707 (m)		CH			
	744	bending			
		modes		794 (w)	
			874 (w-m)	880 (w-m)	
	958		963 (w)	990 (w)	
1027 (m)	1009				
		In-plane		1097 (w)	
		CH		1154 (w0	
1168 (w)	1163	bending		1166 (w-m)	1165 (w)
	1176	modes		1177 (w-m)	
1204 (m)	1209			1194 (w-m)	

* Ordinary Raman spectrum;

** Abbreviations: w=weak; m=medium, s=strong, vs=very strong
a - on C_1 sol without $BaCl_2$, b - on C_1 and c - on C_2, both with $BaCl_2$

1245 (w)			1262 (m)	1265 (s)	1267 (w)
	1270				
1287 (m)	1277			1289 (m)	1285 (w)
1347 (vs)			1355 (m-s)	1354 (s)	1354 (m-s)
1382 (w-m)				1372 (m)	1372 (m)
	1401		1406 (m)	1407 (vs)	1406 (m-s)
1440 (w)	1415			1443 (w)	
			1452 (w)	1452 (w)	
1464 (m)	1463	Ring-stret-			
1480 (s)	1478	ching			
	1514	modes	1520 (w)	1520 (w)	
1539 (m)					
	1556				1558 (m-s)
1560 (s)			1564 (s)	1564 (s)	1564 (m)
	1573				
1600 (m)			1608 (m)	1608 (m)	
			1612 (m)	1612 (m)	
1642 (m-s)					
1700 (w)			1702 (w)	1702 (w)	1702 (w)
1712 (w)					

In the limit of the experimental errors, the peaks position are roughly the same (±4 cm^{-1}) at all values of the potential (see also Fig. 3 b, c, d).

Comparing a and b SERS spectra (Fig. 3) obtained using the same colloid C_1 without (a) and with (b) $BaCl_2$ solution in SERS active system the presence of $BaCl_2$ contributes to the enhancement mechanism without shift the peaks position.

Moreover, the other advantage of the presence of Cl^- in solution is the prevention of the photoreactions on the silver surface [5].

The peaks position in the ordinary Raman spectrum of [9,(10H)A] and in the SERS spectra on C_1 and C_2 colloids are listed in the Table 2. There are also given spectral data of acridine, for comparison.

For the vibrational study of [9,(10H)A], we assumed the b SERS spectrum (Fig. 3) obtained using the C_1 colloid is the best. Futher discussions will refer to this one.

[9,(10H)A] is a plane molecule belonging to C_{2v} symmetry (like acridine and pyridine - the most studied molecule in this field).

According to Brigodiot and Lebas [6], from the 63 vibrations of acridine ($22A_1$, $9A_2$, $11B_1$ and $21B_2$) denoted in terms of Wilson's notation, compared to the 66 vibrations of acridinium ion ($23A_1$, $9A_2$, $12B_1$ and $22B_2$), three of those are νNH A_1, δNH B_2 and γNH B_1.

As a derivative of acridine [7,8], 9,(10H) Acridone presents a different Infrared (IR) and Raman (R) spectrum. These differences can result from the interaction between vibrations of the same and different symmetry, like interactions between the ring stretching modes and bending modes (N-H, C=O).

Out of plane deformation modes of C-H bending* of [9,(10H)A] 750 and 855 from IR (our measurements) are not active in Raman.

In plane C-H bending modes: 1025, 1107, 1123, 1168, 1183 and 1263 from IR are founded in Raman as 1027, and 1168. The last one appears in SERS spectrum as 1166, 1177 doublet.

Ring stretching modes (IR: 1356, 1371, 1476, 1561 and 1602) appear in Raman at 1347 (as the strongest peak), 1480, 1560 and 1600. In SERS spectrum these modes appear at 1354, 1564 and 1608.

Around 1600 in IR spectrum of [9,(10H)A] there is an overlapping between the ring stretching, C=O and N-H modes. Specific for IR at 1636, the C=O bending mode, appears in ordinary Raman at 1642. In SERS spectra in this region a large band is present.

As δNH bending modes there are 1554 and 1600±10 in IR. In ordinary Raman they

* All frequencies in cm^{-1}

appear at 1560 and 1600, which have correspondents in SERS at 1564 (an overlapping with the ring stretching mode), 1608 and 1612. [9,(10H)A] may be adsorbed on the silver surface, via nitrogen lone pair electrons, via its ring π system or via oxygen lone pairs electrons.

It is known that frequencies of ring-stretching vibrations decrease by more than 10 cm^{-1} and their bandwidth increase when molecules adsorb on the silver surface via their π system [5].

Concerning this supposition, the 1560 vibration from ordinary Raman spectrum might be assigned as δNH mode which appears in all SERS spectra constantly blue-shifted to 1564.

This confirms the supposition that [9,(10H)A] is bounded to the silver surface via nitrogen lone pair electrons and also we have the indication that the surface-ring π orbital overlap does not occur significantly when [9,(10H)A] adsorbs on the silver surface. According to the selection rules proposed by Moskovitz [9] and Creighton [10] the vibrational mode with its normal mode component to the metal surface is much more enhanced than the parallel one. In particular, from the SERS spectrum and Table 2 we observe that the ring stretching modes of [9,(10H)A] are more enhanced than the others.

This idea sugests that the plane of the [9,(10H)A] molecule is perpendicular or tilted on the Ag surface.

At a more negative potential of the Ag surface, where SERS spectrum presents large bands (Fig. 3c), we suppose that the π ring electrons have an important role in the adsorption of [9,(10H)A] molecule on the silver surface.

4. Conclusions. The best SERS spectrum was obtained on the C_1 colloid, comparing to that obtained on C_2 and C_3.

The [9,(10H)A] molecule is bounded on the Ag surface via its nitrogen lone pair electrons and oriented with its plane perpendicular or tilted on the surface.

At a more negative potential of the surface, probably the π ring electrons are more involved in the adsorption of the molecule.

References

[1] R.K. Chang, Th.E. Furtak, Surface Enhanced Raman Scattering, Plenum Press, New-York 1982.
[2] M. Moskovits, Mod. Phys. 57, (1993), 3
[3] K. Čermáková, O. Šesták, P. Matějka, V. Baumruk and B. Večková, Chem. Commun. 58, (1993), 2682
[4] A.M. Ahern, R.L. Garrell, Anal. Chem 59, (1987), 2816
[5] S.T. Oh, K. Kim, M.S. Kim, J. of Phys. Chem. 95, (1991), 8844
[6] M. Brigodiot, J.M. Lebas, J. Chim. Phys. Phys. Chim. Biol. 69, (1972), 964
[7] T.Iliescu, I. Marian, R. Mîrca, V. Smarandache, Analyst 119, (1994), 567
[8] T. Iliescu, M. Vlassa, M. Caragiu, I. Marian, S. Astilean, To be published in Vibrational Spectroscopy
[9] M. Moskovits, J. Chem. Phys. 75, (1981), 3126
[10] J.A. Creighton, Surf. Sci. 124, (1983), 209

STUDIA UNIV. BABEŞ-BOLYAI, PHYSICA, XXXIX, 1,1994

OPTICAL ABSORPTION STUDY ON SODIUM-PHOSPHATE GLASSES CONTAINING URANIUM IONS

I.Milea*, V.Simon** I.Ardelean** O.Cozar**, T.Fiat**, L.Daraban**, V.Mih**, D.Beesa**

ABSTRACT. Optical absorption spectra were investigated on $xUO_3 \cdot (1-x)[2P_2O_5 \cdot Na_2O]$ glass system ($0 < x \leq 0.2$), at room temperature, in order to identify the valence states of uranium in these samples. The results evidenced the presence of U^{3+}, U^{4+} and U^{6+} ions. The content of U^{4+} ions depends on UO_3 concentration in glasses.

INTRODUCTION. The uranium is a major component of the nuclear wastes, whose storage implies its immobilization in adequate host materials. Among the materials recommended as proper host for radioactive nuclides the glass matrices are of great interest. The ideal glass would be that in which all the amount of radioactive waste would be ready solved during the glass preparation process and that would assure a good immobilization of the stored ions in a large range of physical and chemical environment conditions.

The possible valence states of uranium ions take values between 2 and 6. According to the valence states the uranium ions are differently soluble in a glass matrix but on the other hand the most soluble ions are not the easiest to be highly stabilized in the same matrix in order to avoid the appearance of a uranium reach surface layer [1-5]. The redox reaction products during the glass melting are allways depending on the glass microstructure. The local order characterizing the oxide glasses is influenced by the nature and share of glass former, glass modifier components and their ratio in the glass matrix. All these aspects impose a large investigation of the glass systems used as radioactive waste storage materials.

* *Technical University of Cluj-Napoca, 3400 Cluj-Napoca, Romania*
** *"Babeş-Bolyai" University, Faculty of Physics, 3400 Cluj-Napoca, Romania*

EXPERIMENTAL

The investigated samples belong to the xUO_3 $(1-x)[2P_2O_5$ $Na_2O]$ glass system with $0 < x \leq 0.2$ mol. The glasses were obtained by melting of UO_3, $(NH_4)_2HPO_4$ and Na_2CO_3 $10H_2O$ powder mixtures of desired concentration in the investigated composition range, in sintered corundum crucibles, at 1250°C for 15 minutes, followed by quickly undercooling at room temperature on stainless steel plates. The crucibles were introduced directly at the preparation temperature in an electrical furnace with superkanthal bars. All samples were light green coloured and the colour was intensified with UO_3 concentration.

Gamma spectrometry data were used to analyse the uranium content in the prepared glasses. The linear dependence of the decay rate (^{235}U) on UO_3 concentration, for the same amount of samples, indicates that the uranium introduced in the powder mixtures was incorporated in the glass samples without losses during the melting process (Fig. 1).

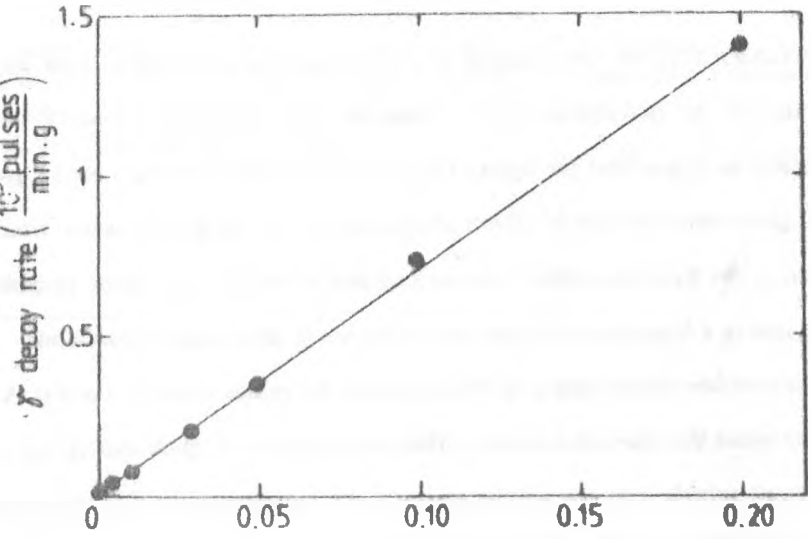

Figure 1. The dependence of gamma decay rate on samples composition for xUO_3 $(1-x)[2P_2O_5$ $Na_2O]$

The optical absorption spectra were recorded on a Specord UV-VIS spectrometer in the wavenumber range 10000 - 30000 cm^{-1}, at room temperature.

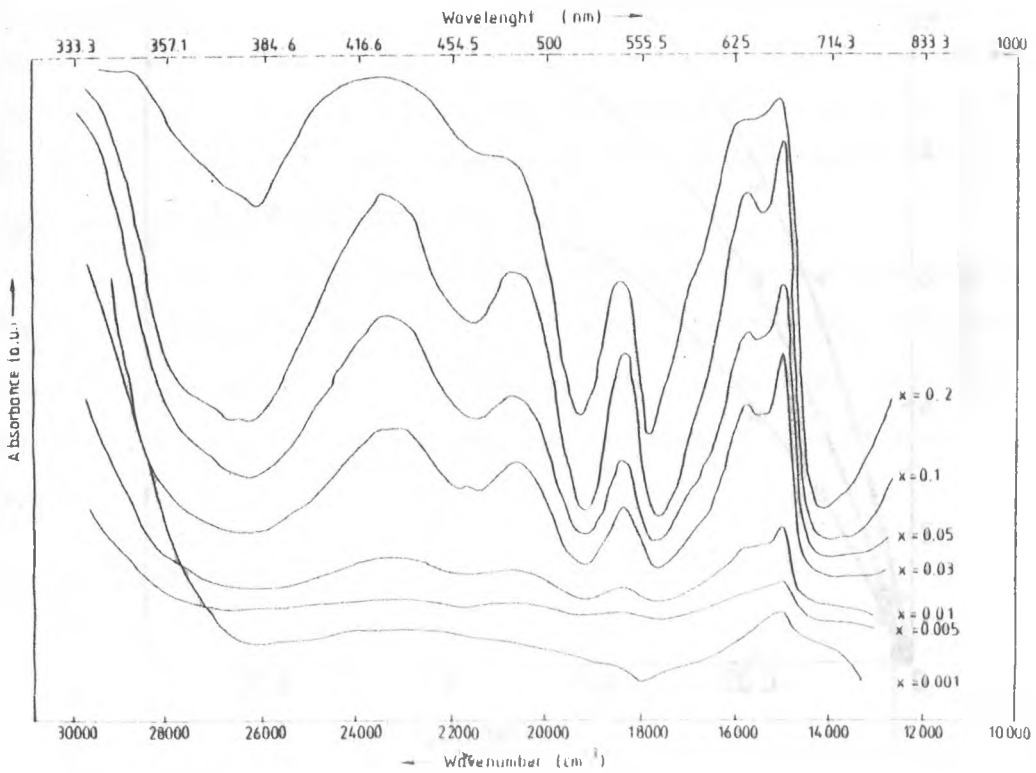

Figure 2 Optical absorption spectra from xUO_3 $(1-x)[2P_2O_5\ Na_2O]$ glasses

RESULTS AND DISCUSSION

As can be seen in figure 2 the optical absorption spectra of the investigated glasses show absorption bands centered on 13800, 15000, 16060, 18200, 20810, 23200 and 27000

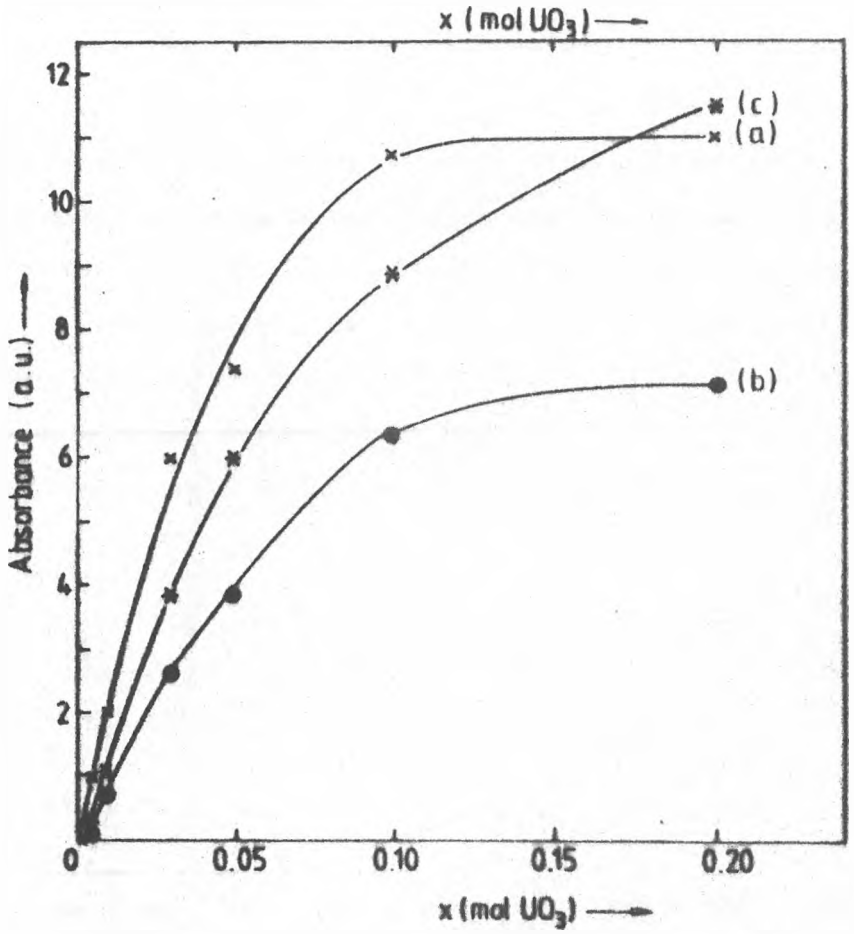

Figure 3 The composition dependence of the relative intensities of 15000 cm^{-1}, 20810 cm^{-1} and 23200 cm^{-1} absorption bands for $xUO_3(1-x)[2P_2O_5 Na_2O]$ glasses.

a cm^{-1} The relative intensities of 15000 cm^{-1} band assigned to U^{4+} ions (curve a, Fig 3) nd of 20810 cm^{-1} band attributed to U^{6+} ions (curve b, Fig 3) are increasing with UO_3 concentration in glasses These dependences are pronounced up to x = 0 1 and they are followed by a smooth shoulder when UO_3 content increases to x = 0.2 The similar

dependences of these U^{4+} and U^{6+} bands may be explained by an increase of U^{4+} and U^{6+} ions number in proportion to UO_3 concentration in the melt samples as a part of high valence state ions are reduced to a lower valence state. The higher intensity of U^{4+} band than that of U^{6+} band denotes a greater number of ions in the lower valence state. The absorption band at 18200 cm^{-1} is assigned [6,7] both to U^{3+} and U^{4+} ions and absorption band of 13800 cm^{-1} is assigned to U^{3+} ions. Curve c in figure 3 illustrates the relative intensity dependence of 23000 cm^{-1} band attributed to eightfold coordinated U^{4+} ions on UO_3 concentration. In this case the dependence is appreciable also in the concentration range $0.10^{a} \times {}^{a}0.20$. The absorption band from 16060 cm^{-1} arises from U^{4+} ions too [1, 8], while the bands around 27000 cm^{-1} could be probably associated with U^{6+} ions. This behaviour could be correlated both with the increase of UO_3 content in samples and with the structural changes induced by higher uranium concentration in the phosphate glass matrix [9].

One also remarks that the position of 23200 cm^{-1} absorption band is slightly shifted (Fig.4) to larger wavenumbers when UO_3 content increases, due to the vecinities deformation of eightfold coordinated U^{4+} ions in the glass matrix. We consider that in the investigated glass system the uranium ions could also behave as glass formers and not only as network modifiers.

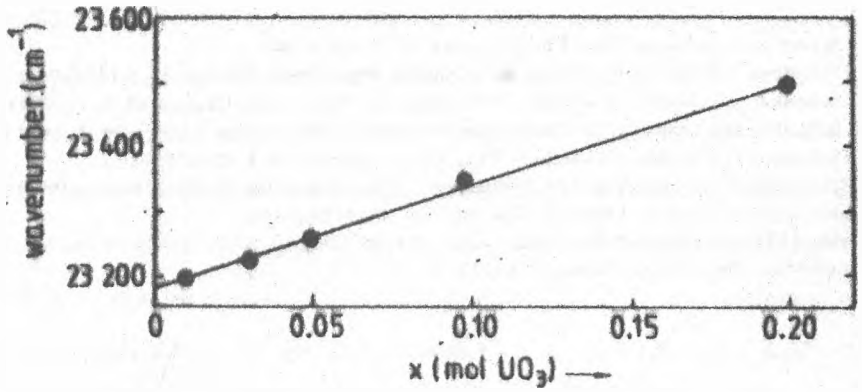

Figure 4 The composition dependence of ~23 200 cm^{-1} band position in xUO_3 $(1-x)[2P_2O_5 \cdot Na_2O]$ glasses.

In borate glasses [1] the U^{6+} ions appear in uranyl UO_2^{2+} radicals, U^{4+} ions are eightfold coordinated and U^{3+} ions are sixfold coordinated. Among the valence states of

uranium ions in glasses U^{4+} is the best stabilized [1] in the melt structure from the point of view of the structural sites. The optical absorption results obtained in this study indicate that a great number of uranium ions introduced in the investigated soda-phosphate matrix was reduced to this valence state

CONCLUSIONS

In the xUO_3 $(1-x)[2P_2O_5$ $Na_2O]$ system, prepared at 1250°C, were obtained glass samples of light green colour in the concentration range $0 < x \leq 0.20$. The optical absorption spectra indicate the presence of uranium ions in 3, 4 and 6 valence state. The majority of uranium ions are in the valence state 4. The absorption band corresponding to octahedrally coordinated U^{4+} ions is shifted to higher wavenumbers when UO_3 content increases in glasses. These results may be correlated with the redox reactions during the sample melting process, with the UO_3 concentration change in samples and with the investigated glass matrix

References

1 H D Schreiber, G.B Balazs, Phys. Chem. Glasses, **23**, 5, 139 (1982)
2 H D Schreiber, G B Balazs, P L Jamison, A.P Shaffer, Phys. Chem. Glasses, **23**, 5.147 (1982)
3. H.D.Schreiber, L M Minnix, G B Balazs, B.E Carpenter, Phys. Chem. Glasses, **25**, 1, 1 (1984)
4 H D Schreiber, B E Carpenter, Y.P.Eckenrode, G.B.Balazs, Phys. Chem. Glasses, **26**, 1, 24 (1985)
5 H D Schreiber, G B Balazs, T.N Solberg, Phys. Chem. Glasses, **26**, 2, 35 (1985)
6 J R Montgomery, J J Fontanella, M C Wintersgill, J. Phys. Chem. Solids, **55**, 2, 201 (1994)
7. E Culea, I Milea, T Iliescu, I Bratu, J. Mat. Sci. Lett. 13, 1171 (1994)
8 E Culea, I.Milea, T Iliescu, J. Non-Cryst. Solids, 175, 98 (1994)
9 J.Krogh-Moe, Phys. Chem Glasses, 2, 46 (1962)

STUDIA UNIV. BABE-BOLYAI, PHYSICA, XXXIX, 1994

RAMAN STUDY OF SOME ALKALI PHOSPHATE GLASSES

T.Ilieșcu,* I.Ardelean, V.Simon, D.Lazar

Received: 15.06.1994

Abstract. The structure of $xNa_2O(1-x)P_2O_5$ glass system with $0 \leq x \leq 0.5$ was investigated by Raman spectroscopy. It was evidenced that the addition of Na_2O determines the breaking of the phosphate chain and the appearance of more pyrophosphate and end units. These structural modifications increase as the Na_2O content increases.

Introduction. The most common glasses are formed by mixing glass forming substances (typically SiO_2, B_2O_3, P_2O_5) with modifier metal oxides [1]. Pure vitreous P_2O_5 is an extremely hygroscopic colourless glass. It was used as an inhibitor of ionic diffusion in oxide layers of silicon devices [2]. New applications in optical fibers seem likely [3]. Sodium-calcium oligophosphate glasses are of special interest both as biomaterials for bone-like protheses with high biological tolerance, their chemical composition being very close to that of bone, and as biomaterials for metallic protheses [4]. It is very interesting to study the structural changes of glasses with their composition and to relate these modifications with their properties. Raman spectroscopy is the tool most widely applied to these structural studies.

Galeener and Mikkelson [5] have used this technique to study the structure of pure vitreous P_2O_5. Short range order in the network of the boro-phosphate glasses determined from Raman spectra was investigated by Scagliotti et al. [6]. Re ently Raman study on

* "Babeș-Bolyai" University, Faculty of Physics, 3400 Cluj-Napoca, Romania

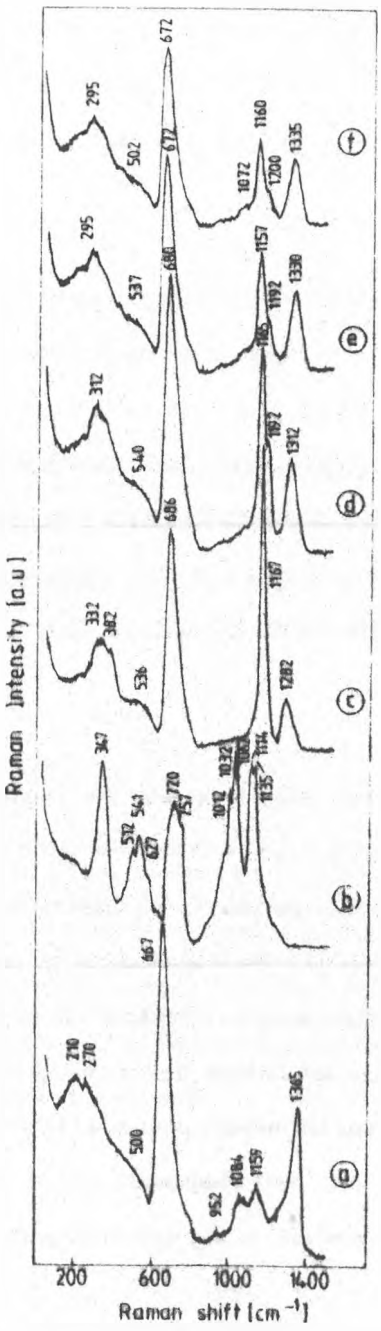

Fig. 1. Raman spectra of $xNa_2O(1-x)P_2O_5$ glasses, (a) x = 0, (b) x = 0.5, (c) x = 0.33, (d) x = 0.25, (e) x = 0.2, (f) x = 0.16

rapidly quenched lithium pyrophosphate glass at various temperatures [7] and structural studies on some boro-phosphate glasses [8] have been carried out. In this paper we present the Raman spectra of $xNa_2O(1-x)P_2O_5$ glass system with $0 \leq x \leq 0.5$ in order to understand the structural changes induced in these glasses by different concentrations of Na_2O.

Experimental. The samples were prepared by mixing of $Na_2CO_3 \cdot 10H_2O$ and $(NH_4)_2HPO_4$ of reagent grade purity and melting the corresponding mixtures ($0 \leq x \leq 0.5$) in sintered corundum crucibles at 1123 K for 10 minutes. For $x \geq 0.57$ we could not obtaine vitreous sample. The melts were poured in parallelipipedic stainless steel forms at room temperature.

The Raman spectra have been recorded on a GDM 1000 double monocromator instrument equipped with ILA 120-1 argon-ion laser. The emission line at 488 nm was used for excitation with power of about 0.6 W. A 90^0 geometry and spectral width of 2 - 3 cm^{-1} were chosen for collecting the scattered light. The spectra were recorded without polarizer in the gathering optics. The measurements were carried out at room temperature.

Results and discussion. The investigated glass system was prepared in the above mentioned conditions because we observed that at lower melting temperatures (723-973K) P_2O_5 glass samples present a strong yellow fluorescence which perturbs the registration of Raman spectra. At higher melting temperatures the fluorescence is quenched. The same fluorescence effects were also observed for P_2O_5 glass samples prepared at different melting temperatures by other authors [5].

Fig.1 shows the Raman spectra of $xNa_2O(1-x)P_2O_5$ glasses with $0 \leq x \leq 0.5$. Our Raman spectrum of pure vitreous P_2O_5 is the same as that recorded by Galeener and Mikkelsen [5]. This spectrum indicates that the pure phosphate glass is a continuos random network (linear polymeric structure) of quasi-tetrahedral PO_4 units (phosphorous is four coordinated) in which only three of the oxygen atoms of each unit bridge to neigbouring units, while the fourth is doubly bounded to the central phosphorous atom.

The presence of the modifier decreases the number of bridging oxygens in PO_4 units, while its negative charge increases. In connection with increasing negative charge [6] the phosphate units are:

- the neutral "branching unit" with three bridging oxygen and one double P = 0 bond

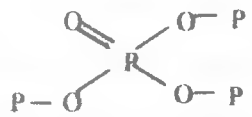

- the "middle unit", often called the metaphosphate unit (- O - PO_2-O):

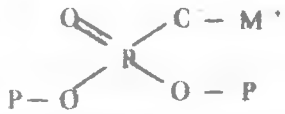

(M = modifier atom)

- the "end unit" $\left(-O - PO_3^{2-}\right)$

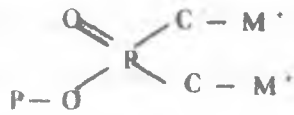

- the monomer or ortophosphate unit, with four non bridging oxygens $\left(PO_4^{3-}\right)$:

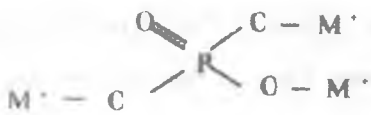

Raman spectra of phosphate glasses are determined by vibration of these units. Figure 2 presents some of vibrational modes in the phosphate units

The peaks position and assignment of Raman lines obtained for the investigated glasses are presented in Table 1. The assignments were made by comparison with other phosphate glasses [3-8].

As we can see from figure 1 a and Table 1 in Raman spectrum of pure P_2O_5 glass the dominant bands are centered at 667 and 1365 cm^{-1} and they were ascribed to symmetric P-O-P stretching and P = O stretching vibrations, respectively. With increasing of Na_2O concentration the band at 1365 cm^{-1} decreases in intensity and changes its position to lower wave number (Fig 3). This indicates, on the one hand, the decrease of branching units with three bridging

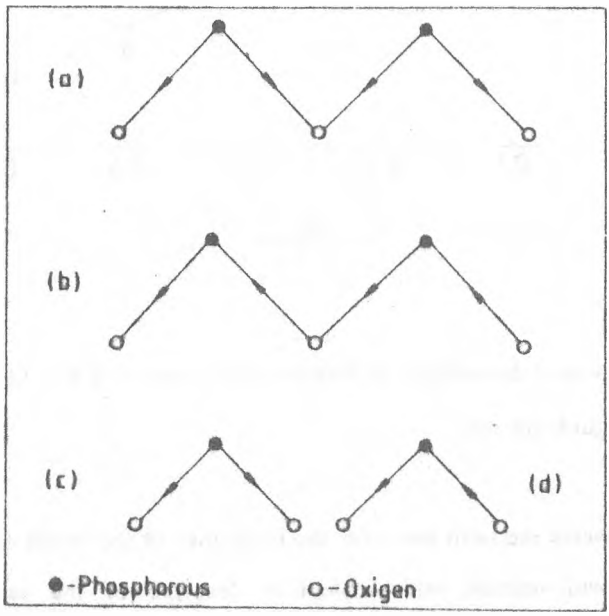

Fig. 2. Vibrational modes in phosphate units: (a) symmetric P-O-P stretch, (b) asymmetric P-O-P stretch; (c) symmetric -O-P-O- stretch, (d) asymmetric -O-P-O- stretch.

oxygens and, on the other hand, the increase of the strength of P = O bond with increasing of Na_2O concentration. The band centered at 667 cm^{-1} in pure P_2O_5 glass (x = 0) slowly shifts to higher wave numbers with increasing Na_2O content and for the sample with x = 0.5 it is centered at 720 cm^{-1}.

At the same time the intensity of the band centered at ~1160 cm^{-1} is amplified with rising Na_2O concentration and its position remains practically unchanged in the investigated composition range. However one observes a weak shift to 1135 cm^{-1} for x = 0.5.

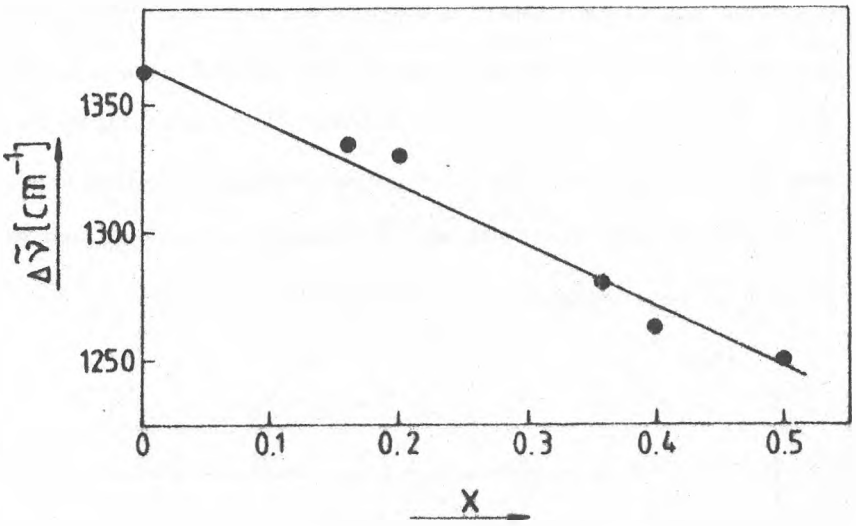

Fig. 3. The composition dependence of Raman peak position of P = O stretching vibration. The line is only a guide for eye.

Fig. 4 presents the ratio between the intensities of the bands centered at 670 cm^{-1} and 1165 cm^{-1} versus natrium oxide content. A decrease of the ratio I_{670}/I_{1165} with increasing Na_2O concentration was observed and this can be explained by the growth of metaphosphate units number. In this way the number of nonbridging oxygens is rising in the glasses whereas the Na_2O content increases. In the sample with the highest content of Na_2O ($x = 0.5$) the intense bands are developed at 1012 - 1032 cm^{-1} and 1114 - 1135 cm^{-1} and they are related to P-O stretching vibration within the end groups and within the middle units respectively. This means that for $x = 0.5$ the polyphosphate chains are further brooken and a greater number of middle and end units appears.

A very weak band around 950 cm^{-1} is observed in the Raman spectra of all investigated samples. We assign this band to PO stretching vibration in monomer units which are present in a very small amount even in the pure P_2O_5 glass. In the "free" ion the total symmetric vibration is expected at 980 cm^{-1} [6]. A very intense band at 1062 cm^{-1} observed

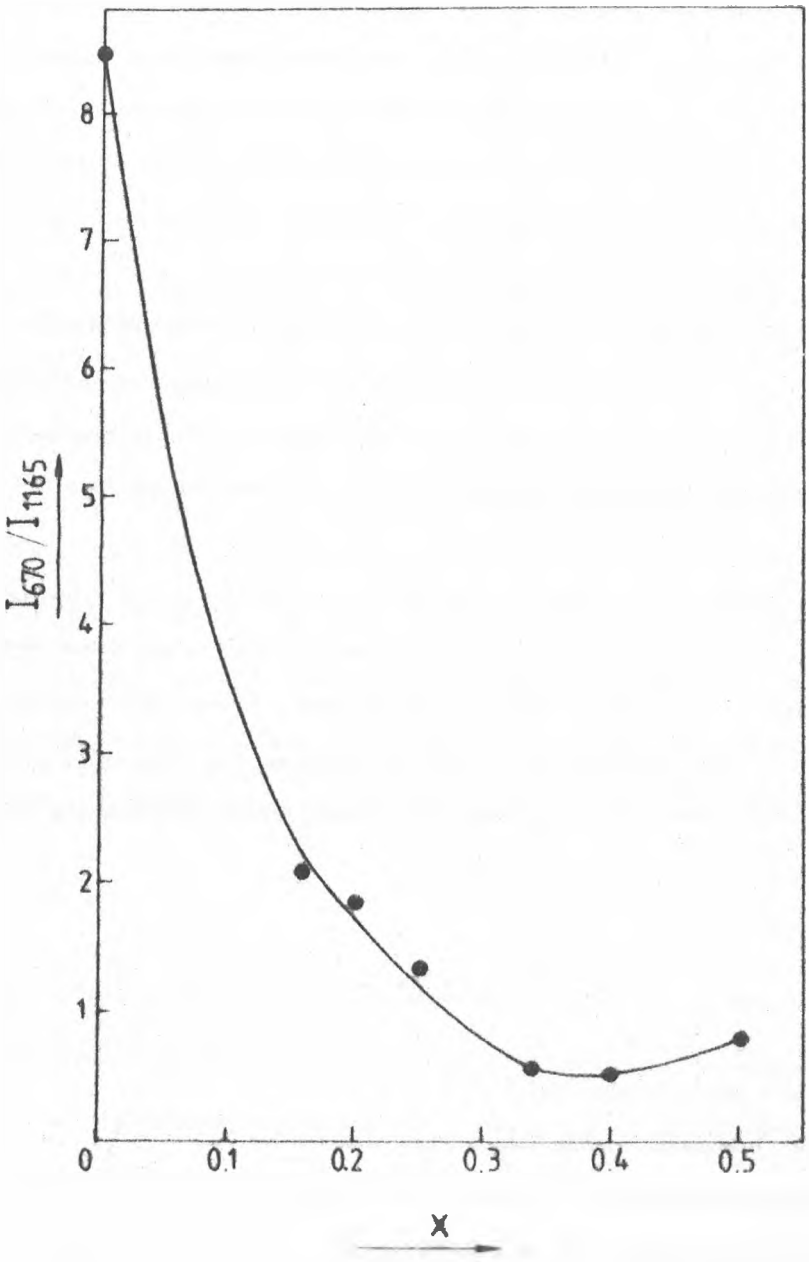

Fig 4 I_{670}/I_{1165} dependence on Na_2O content in $xNa_2O(1-x)P_2O_5$ glasses The line in only a guide for eye

in the sample with x = 0.5 can be assigned to PO stretching vibration in pyrophosphate units $(P_2O_7^{4-})$. In lithium phosphate glasses this vibration is observed at 1050 cm^{-1} [7].

The comparison of Raman spectra of lithium phosphate glasses [6] with the Raman spectra of our natrium phosphate glasses indicates that the breaking of polymerization chain is produced at a lower Na_2O than Li_2O concentration. Approximately the same bands were observed in lithium phosphate glasses for x = 0.62 and in our glasses for x = 0.5. This result is probably due to the difference in the dimensions of lithium and natrium ions.

In the Raman spectrum of Na_2O P_2O_5 glass sample an intense band in the range 512-627 cm^{-1} occurs which we can not yet attribute to a certaine vibration and also occurs an other intense band at 347 cm^{-1} which could be ascribed to O-P-O rocking units (Table I). Further studies are necessary in this case.

Conclusions. The Raman study that we carried out in this work leads to the conclusion that the addition of O Na_2 modifier to P_2O_5 glass former determines a depolymerization of the three dimensional P_2O_5 vitreous network and the appearance of a larger numbers of pyrophosphate, middle and end units. The breaking of polymerization chain is produced at a lower Na_2O than Li_2O concentration in phosphate glasses containing natrium oxide and lithium oxide, respectively.

References

1. D Ravaine, J. Non-Cryst. Solids, **73**, 287 (1985)

2. E.A.Coni, S L.Silverman, Y S.Kim, Solid State Electronics **9**, 1009 (1966)

3. F L.Gallener, J.C.Mikkelsen jr , R H Geils, W J.Mosby, Appl. Phys. Lett. **32**, 34 (1978)

4. A.Bertoluzza, M A Battaglia, R Simoni, D A Long, J. Raman Spectrosc. **14**, 178 (1983)

5. F L.Gallener, J.C.Mikkelsen jr., Solid State Commun. **30**, 505 (1979)

6. M Scagliotti, M Villa, G.Chiodelli, J. Non-Cryst. Solids **93**, 350 (1987)

7. Y.Kowada, H Adachi, M Tatsumisago, T .Minami, Phys Chem Glasses **34**, 10 (1993)

8. J F Dual, J J Vidlan, M.Couzi, Phys. Chem. Glasses **34**, 212 (1994)

STUDIA UNIV. BABEŞ-BOLYAI, PHYSICA, XXXIX, 1, 1994

LOW TEMPERATURES MAGNETIC PROPERTIES OF $Gd_xY_{1-x}Co_{12}B_6$ COMPOUNDS

I. LUPŞA* and P. LUCACI*

Received: 10.01.1994

ABSTRACT. - The magnetic properties of $Gd_xY_{1-x}Co_{12}B_6$ compounds were studied in the temperature range 4.2-300 K and fields up to 70 kOe. The compound $YCo_{12}B_6$ is ferromagnetically ordered. In $Gd_xY_{1-x}Co_{12}B_6$ an antiparallel coupling of gadolinium and cobalt magnetizations is evidenced.

1. Introduction. In order to search new permanent magnetic materials several studies on the magnetic behaviour of $RCo_{12}B_6$ systems were performed (R is a rare earth or yttrium) [1-3]. The crystal structure for these compounds is reported [1] as a rhombohedral one, of $SrNi_{12}B_6$ type (space group R3m). The magnetic measurements released that Co moments couple antiferromagnetically with Gd moments. The compensation temperature for $GdCo_{12}B_6$ is 48 K. The Curie temperatures are 178 and 162 K for compounds with Y and Gd respectively [1,2].

2. Experimental. The $Gd_xY_{1-x}Co_{12}B_6$ samples were melted in an arc furnace in a purified argon atmosphere. They were thermally treated in vacuum for 3 weeks at 800 °C.

Magnetic measurements were performed in the temperature range 4.2-300 K and fields up to 70 kOe. The spontaneous manetizations M_s were determined from the magnetization isotherms according to the approach-to-saturation law $M = M_s(1 - a/H) + \chi'_{as} H$ where a is the

* *Technical University, 3400 Cluj-Napoca, Romania*

coefficient of magnetic hardness and χ_0 is the field independent susceptibility.

3. Results and discussion. The results of magnetization measurements performed at 4.2 K are presented in figure 1. It is seen a tendency towards saturation in fields of 20 kOe for all compounds.

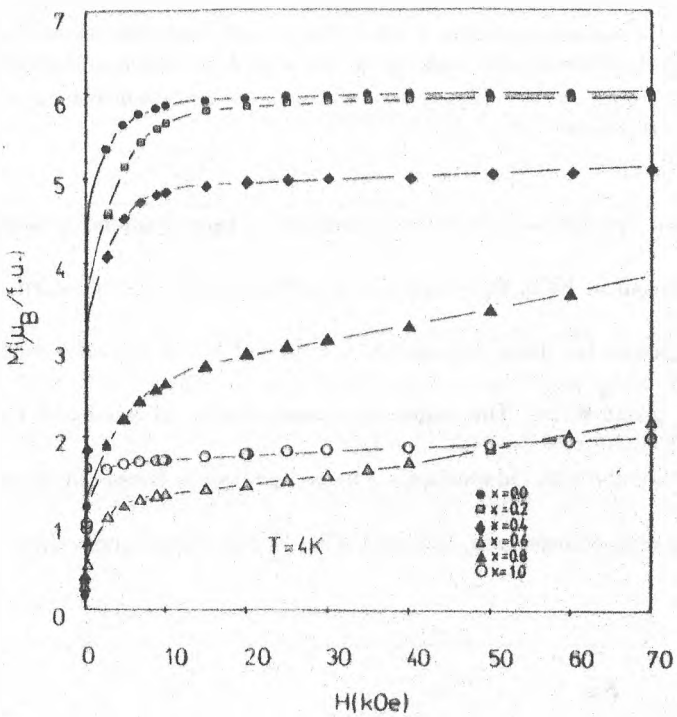

Fig. 1. The 4.2 K magnetization isotherms of $Gd_xY_{1-x}Co_{12}B_6$ systems.

From the magnetization isotherms performed at several temperatures the spontaneous magnetizations were determined. We present in figure 2 the thermal dependence of magnetizations for $Gd_xY_{1-x}Co_{12}B_6$ compounds.

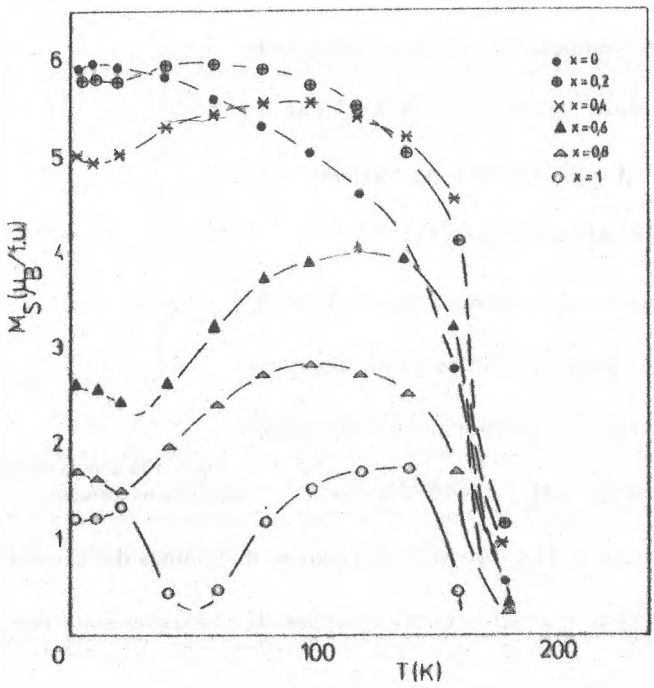

Fig.2. The thermal variations of spontaneous magnetizations for $Gd_xY_{1-x}Co_{12}B_6$ compounds

The compound $YCo_{12}B_6$ is ferromagnetically ordered having the Curie temperature at 178 K in good agreement with previously determined values [1-3] The magnetic behaviour of $GdCo_{12}B_6$ system indicates an antiparallel coupling between Co moments and Gd respectively, with the compensation temperature of 48 K and a Curie temperature of 162 K These results are close to those previously reported

All intermediate systems present a ferrimagnetic ordering with compensation temperatures increasing from 15 K for x=0 2 to 48 K corresponding to $GdCo_{12}B_6$. The composition dependence of compensation temperatures plotted in figure 3 shows an almost linear increasing when gadolinium content is greater.

The Curie temperatures of these compounds are situated between 162 K and 178 K. These T_c values of $Gd_xY_{1-x}Co_{12}B_6$ systems are relatively low as compared with RCo_4B systems [4].

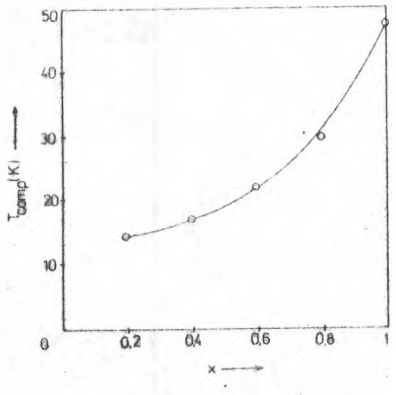

Fig.3. The composition dependence of compensation temperatures for $Gd_xY_{1-x}Co_{12}B_6$ alloys

The spontaneous magnetization in $YCo_{12}B_6$ is due to cobalt magnetic lattice (5.9 μ_B/f.u.). As yttrium is substituted by gadolinium an antiparallel coupling of Gd magnetization with the cobalt moments is developed. The increasing Gd content determines the decreasing of spontaneous magnetization and an increasing of the compensation temperatures from 15 K to 48 K.

References

1. M.Jurczyk, A.T.Pedziwiatr, W.E.Wallace, J.Magn.Magn.Mater. 67,11,1987
2. M.Mittag, M.Rosenberg, K.H.J.Buschow, J.Magn.Magn.Mater. 82,109,1989
3. G.F.Zhou, X.Li, F.R.de Boer, J.Magn.Magn.Mater.109,265,1992
4. A.T.Pedziwiatr, S.Y.Jiang, W.E.Wallace, E.Burzo, V.Pop, J.Magn.Magn.Mater. 66,69,1987

STUDIA UNIV. BABEŞ-BOLYAI, PHYSICA, XXXIX, 1, 1994

INTRA- AND INTERGRAIN EFFECTS OF THE PARTIAL SUBSTITUTION OF Cu BY SOME 3d ELEMENTS IN THE "2223" SUPERCONDUCTOR

A.V.POP*, I.I.GERU**, V.G.KANTSER***, D.CIURCHEA*, L.PAVEL*, Gh.ILONCA*

Received: 7.02.1994

ABSTRACT. - Electrical resistivity and d.c. susceptibility measurements were performed on the "2223" superconductor after a 2 at. % partial substitution of Cu by Cr and Mn. The changes in residual resistivity $\rho(0)$ and in $d\rho/dT$ are in agreement with the decrease of T_c. The linear correlation between the decoupling temperature T_d and the magnetic field (H<150e) characterizes the intergrain junctions.

1. INTRODUCTION. The superconductivity in the high-T_c cuprates is usually supressed by the substitutional elements in the CuO_2 planes. The origin of the decrease in T_c by point defects created by replacing the Cu atoms by other 3d elements is not very clear yet. Candidates for the supression of T_c are an indirect magnetic process of the Abrikosov-Gorkov type on the magnetic Cu moments induced by the dopants [1] or a nonmagnetic elastic scattering process [2]. The systematic variation of the fundamental properties for as many high T_c superconductors as possible is desirable in order to separate the correlations common to all oxide superconductors. The change of the normal electric resistivity when the point defects are introduced into the CuO_2 planes can yield informations on the interaction of the charge carriers with the impurity. In the granular HTS superconductor with weak links between the grains, the intergrain supercurrent can be partially supressed under such

* *"Babeş-Bolyai" University, Faculty of Physics, 3400 Cluj-Napoca, Romania*

** *Moldova State University, Faculty of Physics, 277014 Chişinău, R.Moldova*

*** *Institute of Applied Physics, 277028 Chişinău, R.Moldova*

conditions as high transport currents or external magnetic field. The decoupling temperature T_d when the intergrain supercurrent ceases to flow shifts to lower temperature on increasing the aplied magnetic field [3,4].

In this paper we report an investigation of the effect of the partial substitution of Cu by Cr and Mn in the "2223" superconducting system on the electrical resistivity and the decoupling temperature.

2. EXPERIMENTAL. The bulk samples of nominal composition $(Bi_{1.6}Pb_{0.4})(Sr_{1.8}Ba_{0.2})Ca_2(Cu_{0.98}M_{0.02})O_y$ where M=Cr,Mn were prepared by the conventional solid state reaction [5]. The qualitative X-Ray diffraction analysis performed with a DRON-2 equipment confirmed the predominant "2223" phase, i.e. 95% and 90% in the Cr and Mn samples respectively. The presence of about 5% "2212" phase was detected in both samples along with a little amount of Ca_2PbO_4 in the Mn doped sample.

The electrical resistance was measured by the standard four lead technique between 77 and 290 K [6].

A SQUID-based magnetometer provided the magnetisation as a function of the applied magnetic field and of the temperature T.

3. RESULTS AND DISCUSSION. Above the paraconductive region, in the 170-290 K temperature range, the samples are characterized by a linear temperature dependence of the electrical resistivity :

$$\rho = \rho(0) + a \cdot T$$

Table 1. The values of ρ(0) and a=dρ/dT obtained from the linear fit, and the critical temperatures T_{cm} obtained from the excess conductivity analysis [5,6].

Sample M	ρ(0) [10^{-4} Ω·cm]	dρ/dT [10^{-6} Ω·cm/K]	T_{cm} [K]
0.02 Cr	2.48	4.86	107.6
0.02 Mn	3.99	9.8	105.8

The change of dρ/dT (Table 1.) may be due to the changes in the charge-carrier concentration [7]. The increase of ρ(0) can be explained in terms of the increasing scattering of the charge carriers on the 3d impurities. In Anderson's model of the linear resistivity [8] a dopant in the CuO_2 planes is expected to induce a temperature independent magnetic-scattering rate. In this model, the change in dρ/dT can be interpreted as a change of the magnetic fluctuations yielded by the point defects in the CuO_2 planes.

Another effect of the magnetic 3d impurities on the superconductivity is the reduction of T_c from 108 K in the undoped sample [6] to 107.6 and 105.8 in Cr and Mn doped samples respectively.

In the first set of the magnetic measurements, the sample was cooled from 140 K down to 5 K in zero field (ZFC), when a magnetic field in the range 6.5-13 Oe was applied. The corresponding ZFC susceptibility is $\chi = -\frac{1}{4\pi}$, if the induced supercurrent density J is smaller than the intergrain critical current density $J_{c(intergr)}$. The susceptibility corrected for demagnetizing effects is $\chi = M(H-4\pi DM)$, where M=m/V is the magnetization, V is the geometrical volume and D is the demagnetizing factor. An approximate value D=0.195 was taken into account for all samples, which have the same elongated shape and the same mass [9].

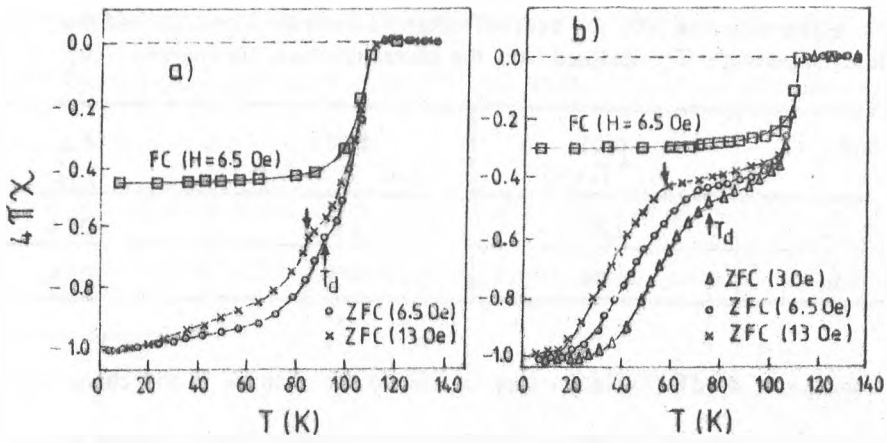

Figure 1. The magnetic susceptibility data of the "2223" samples for the 2 at. % Mn (a) and 2 at. % Cr (b) in field cooled FC) and zero field cooled (ZFC).

Fig. 1.a and Fig. 1.b show the results of the ZFC measurements vs. temperature in the x=0.02 Mn and Cr samples respectively. Two successive transitions at T_c and a 'shoulder' at the decoupling temperature T_d are observed. The latter is strongly dependent on the magnetic field value. This behaviour is attributed to the weak links at the grain boundaries. With increasing temperature, the intergrain supercurrent $J_{c(inter)}$ decreases and the external field penetrates the intergrain weak links. As a consequence of the rapid decrease of $J_{c(inter)}$ with increasing the magnetic field, the position of the 'shoulder' moves to lower temperatures.

In Fig. 2. we show the dependence of the decoupling temperature T_d vs. H for the "2223" with x=0.02 Cr and Mn respectively. The decoupling temperature T_d apparently linearly increases as H decreases with the slopes dT_d/dH=-1.43 K/G for Mn and -0.83 K/G for Cr. This indicates that the partial substitution of Cu by Cr and Mn differently influences the intergrain critical current desity of the Josephson junctions. The presence of the magnetic

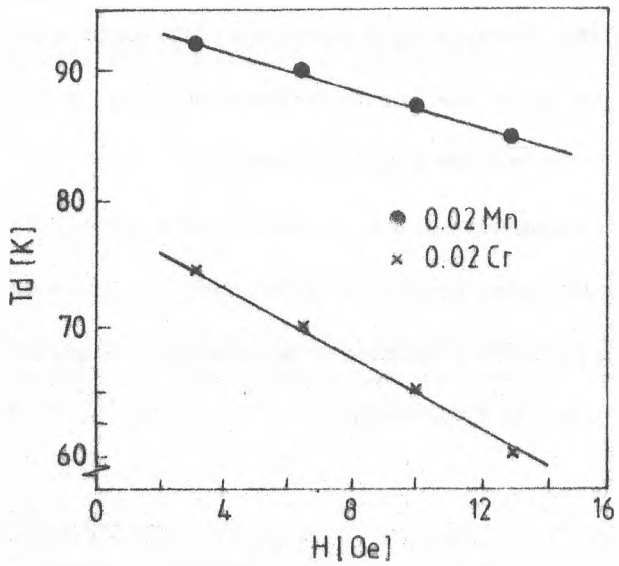

Figure 2. The dependence of the decoupling temperature T_d vs. the applied magnetic field for the "2223" samples 2 at. % doped with Mn (⊙) and Cr (x).

moment of Cr or Mn at these junctions yields a variation of the effective value of the magnetic field.

The Meissner effect was measured in an external field of 6.5Oe by cooling the sample from 140 K (FC). In these measurements (Fig. 1.a and b) the absence of the 'shoulder' is obvious. The bulk Meissner effect was incomplete, yielding $4\pi\chi = -0.29$ and -0.45 in the Cr and Mn doped samples respectively. These results suggest that in the Cr doped sample the flux pinning by the defects within the grains is larger comparatively to the Mn doped sample. The significant difference between the magnetic susceptibilities measured in field cooled and zero field cooled is typical for the porous multiconnected superconductors with a large quantity of pinning centers.

4. CONCLUSIONS. The temperature dependence of the electrical resistivity is linear above the paraconductive region. The partial substitution of Cu by Cr and Mn differently affects the residual resistivity $\rho(0)$, the slope $d\rho/dT$ and T_c.

The magnetization measurements indicate that the grains of the "2223" doped sample are weakly linked. The decoupling temperature of the grains T_d, shows a linear dependence on slight magnetic fields ($H<15Oe$). The slope of this dependence is smaller in the Cr doped sample comparatively to the Mn doped sample.

REFERENCES

1. A.M.Finkelstein, V.E. Kateaev, E.F. Kutovskil, G.G. Teitelbaum, Physica C, 168, 370(1990).
2. J.F. Foulkes, B.L. Gyorffy, Phys. Rev. B, 15 , 1395(1977).
3. J.R. Thomson, J. Brynestad, D.M. Kroeger, Y.C. Kim, S.T. Sekula, D.K. Christen, E.D. Specht, Phys Rev. B, 39, 6652(1989).
4. R.S. Liu, S.Y. Lin, K.N. Tu, P.P. Edwards, W.Y. Liang, Physica C, 185-189,1805(1989).
5. A.V. Pop, Gh. Ilonca, D. Ciurchea, V. Pop, I.I. Geru, submitted to Balkan Physical Letters (1994).
6. A.V. Pop, Gh. Ilonca, D. Ciurchea, V. Pop, L.A. Konopko, I.I. Geru, M. Todică, V. Ioncu, Int. J. of Mod. Phys. B , (1994)-in press.
7. B. von Hedt. W. Lisseck, K. Westerholt, H. Bach, Phys. Rev. B, 49, 9898(1994).
8. P.W. Anderson, Phys. Rev. Lett., 67, 2092(1991).
9. Z.L. Wang, J. Brynestad, D.M. Kroeger, Y.R. Sun, J.R. Thomson, R.K.Williams, Phys. Rev. B, 48, 9726(1994).

STUDIA UNIV. BABEŞ-BOLYAI, PHYSICA, XXXIX, 1, 1994

DIFFEOMORPHISM COHOMOLOGY IN 2D CONFORMAL GRAVITY

I. TATARU*, I.V. VANCEA* and A. BLAGA**

Received: 20.04.1994

ABSTRACT. - We calculate all elements of the BRST cohomology group for the two dimensional conformally invariant gravity. Then, using the operator δ , introduced by Sorella [1], we can solve the descent equation and find out all classical local actions and all candidate anomalies.

1. INTRODUCTION. The most efficient way to study the quantization and renormalization of the gauge (local) theories is given by the BRST transformation and the BRST cohomology [2,3,4]. The gravity can be also introduced as a gauge theory associated with local Lorentz invariance [5] but its action has a different structure which when is put into the shape of a Yang-Mills theory rises the topological quantum field theory [6]. However, in the BRST quantization framework the structure of the invariant action, the anomalies and the Schwinger terms can be obtained in a purely algebraic way by solving the BRST consistency conditions in the space of the integrated local field polynomials. This fact has been known since the work of Wess and Zumino and for a general gauge theory the general form of these can be elegantly formulated in the BV formalism [3,4]. In this framework the Wess-Zumino consistency condition can be written as:

$$sA=(S,A) \tag{1}$$

where S is the proper solution of the master equation, A are integrated local functionals. The

* *"Babeş-Bolyai" University, Faculty of Physics, 3400 Cluj-Napoca, Romania*

** *"Babeş-Bolyai" University, Faculty of Mathematics and Computer Science, 3400 Cluj-Napoca, Romania*

solution of (1) modulo the exact forms can be organized as an Abelian group $H(s)$, the BRST cohomology group. We can introduce a degree in this group by the ghost number and we can decompose it in a direct sum of subspaces with a definite ghost number:

$$H(s)=\oplus H^g(s) \tag{2}$$

Anomalies are represented by cohomology classes of $H^1(s)$ but often it is useful to compute $H^g(s)$ for other values of g as well since H^0 contains the BRST invariant action and H^2 contains the Schwinger terms. Besides, the whole cohomology group could play an important role in solving and understanding the descent equations and in the study of structure of the field configurations.

In this paper we investigate the structure of the entirely cohomology group for a class of two dimensional models which are conformally invariant at the classical level and which shall be characterized throughout of this paper by the field content and the gauge invariance of the theory. Since we try to obtain $H(s)$ for a general framework independent on the local classical action no anti-field structure is introduced.

2. THE MODEL. The fields of our theory are the components of the two dimensional metric $g_{\mu\nu}=g_{\nu\mu}$ and the set of bosonic scalar matter fields ($X=X^A$, $A=1,...,D$). It is convenient to replace the metric by the zweibein fields $e^a{}_\mu$ such that

$$g_{\mu\nu}=e^a{}_\mu e^b{}_\nu \eta_{ab} \tag{3}$$

where $\mu\nu = 0,1$, $a,b = 0,1$, $\eta_{ab}=(+,-)$ or by the moving frame

$$e^a=e^a{}_\mu dx^\mu \tag{4}$$

The conformal properties of the two dimensional space-time are most conveniently described

in terms of light-coordinates

$$x^{\pm}=\frac{1}{\sqrt{2}}(x^0\pm x^1) \tag{5}$$

and the differential operators

$$\frac{\partial}{\partial x^{\pm}}=\frac{1}{\sqrt{2}}\left(\frac{\partial}{\partial x^0}\pm\frac{\partial}{\partial x^1}\right) \tag{6}$$

in the light-cone coordinates the 2D metric can be expressed as a function of the gauge fields

$$h_{\pm\pm}=\frac{g_{\pm\pm}}{g_{+-}+\sqrt{g}} \tag{7}$$

with $g=|\det(g_{\alpha\beta})|$. The gauge fields are inert under the Weyl transformation $g\to e^{\omega}g_{\alpha\beta}$ and they are very convenient when we want to find out different quantities in the framework of a conformal invariant theory.

The BRST transformations of the X and h fields have been obtained in [7](see also [8,9,10]) and they have the form

$$\begin{aligned} sh_{++}&=\partial_+c^-h_{++}\partial_-c^-+c^-\partial_-h_{++}\\ sh_{--}&=\partial_-c^+h_{--}\partial_+c^++c^+\partial_+h_{--}\\ sX&=c^+D_+X+c^-D_-X \end{aligned} \tag{8}$$

where

$$\begin{aligned} D_+X&=\frac{1}{1-y}(\partial_+-h_{++}\partial_-)X\\ y&=h_{++}h_{--} \end{aligned} \tag{9}$$

One can easily obtain the BRST transformations of the ghosts $c^{\pm}$ imposing the condition of nilpotency of the BRST differential and taking into account the fact that it commutes with the operators defined in Eq.(6). After a simple algebraical calculus one gets

$$sc^{\pm}=c^{\pm}\partial_{\pm}c^{\pm} \tag{10}$$

In the framework of the BRST transformations, the search for invariant Lagrangian

anomalies and Schwinger terms can be done in a purely algebraic manner, by solving the BRST consistency condition in the space of integrated local polynomials [4,11,12] This amounts to study the nontrivial solutions of the equation

$$sA=0 \tag{11}$$

where A is an integrated local functional. The condition (11) translates into the local descent equation [11]:

$$\begin{aligned} s\omega_2+d\omega_1&=0\\ s\omega_1+d\omega_0&=0\\ s\omega_0&=0 \end{aligned} \tag{12}$$

where ω_2 is a 2-form with $A=\int\omega_1$, ω_1,ω_0 being local 1-forms, respectively 0-forms It is well known [12,13,14,15,16] that the descent equations terminate in the bosonic string or the superstring in Beltrami or super-Beltrami parametrization always with a non-trivial 0-form and that their integration is trivial

$$\omega_1=\delta\omega_0 \qquad \omega_2=\frac{1}{2}\delta^2\omega_0 \tag{13}$$

where δ is the operator introduced by Sorella [1] and it allows to express the exterior derivative d as a BRST commutator,i e ,

$$d=-[s,\delta] \tag{14}$$

and ω_0 is a solution of the last equation of (12)

$$s\omega_0=0 \tag{15}$$

The main purpose of the present paper is to solve the descent equations (12) in the algebra of the local polynomials of all fields and their derivatives Σ A basis of this algebra can be chosen to consist of

$$\{\partial^p_+\partial^q_-\psi,\partial^p_+\partial^q_-c^+\} \tag{16}$$

where $\psi=(X,h_{\mu\nu},h_{\mu})$, $p,q=0,1,2,\ldots$ However the BRST transformations of this basis are quite complicated and contain many terms which can be eliminated in the cohomology group. In the next section we shall eliminate a part of this basis and introduce a new basis in which the action of the BRST differential is quite simple.

3. THE ALGEBRA. The calculation of the cohomology group can be considerably simplified if we take into account the fact that Σ is a free differential algebra and make use of a very strong theorem due to Sullivan. A free differential algebra is an algebra generated by a basis and endowed with a differential. The Sullivan's theorem states the following:

The most general free differential algebra Σ is a tensor product of a contractible algebra and a minimal one.

A minimal differential algebra M with a differential s is one for which $sM\subset M^{+}M^{+}$ being the part of the minimal algebra in positive degree, i. e. $M=C\oplus M^{+}$ and a contractible differentiable algebra C is one isomorphic to a tensor product of algebras of the form $\Lambda(x,sx)$.

On the other hand, due to Kunneth's theorem the cohomology of a free differentiable algebra is given by the cohomology of its minimal part and we can say that the contractible part can be neglected in the calculation of the cohomology group.

In our case, the construction of contractible and minimal part is straightforward and we do not need any general method to accomplish that. In fact, it is easy to see from the BRST transformations of $h_{\mu\nu},X,c^{*}$ that the generators

$$\partial^p_{-}\partial^n_{-}c^{+},\partial^p_{-}\partial^n_{-}c^{-} \tag{17}$$

with p=0,1,2,... n=1,2,... can be replaced by

$$\{\partial^p_{-}\partial^q_{-}X,\partial^p_{-}\partial^q_{-}\phi,s\partial^p_{-}\partial^q_{-}\phi,\partial^p_{-}c^{+}\} \tag{18}$$

The Sullivan decomposition can be easily obtained from (18). Indeed, the contractible subalgebra generated by

$$\{\partial^p_{-}\partial^q_{-}h_{++},s(\partial^p_{-}\partial^q_{-}h_{++})\} \tag{19}$$

and the minimal subalgebra is generated by:

$$\{\partial^p_{-}\partial^q_{-}X,\partial^p_{-}c^{+}\} \tag{20}$$

This basis is not convenient since the BRST differential has a complicate action on it. The investigation of the BRST cohomology is considerably simplified by using an appropriate new basis which substitutes the fields (X,c^{+}) and their derivatives. The construction of this new basis represents a crucial step towards the calculation of the cohomology group. This new basis has been proposed by Brandt, Troost and Van Proyen in [14] and it is basically intended to substitute one by one the elements of the basis (20) by:

$$\Delta^p_{-}\Delta^q_{-}X=X^{p,q} \tag{21}$$

$$\frac{1}{(p+1)!}\Delta^{p+1}_{-}c^{+}=c^{p}_{+} \tag{22}$$

where

$$\Delta_{+}=\{s,\frac{\partial}{\partial c^{+}}\}=s\frac{\partial}{\partial c^{+}}+\frac{\partial}{\partial c^{+}}s \tag{23}$$

The remarkable property of the new basis is the fact that its BRST transformation is given by the Virasoro algebra with associated ghosts just c^{+}. Indeed, The last two equations (22) and (23) can be rewritten as:

$$sX^{p,q}=\sum_{k\geq 1}(c^k{}_+L^+{}_k+c^k{}_-L^-{}_k)X^{p,q}$$
$$sc^k{}_\pm=\frac{1}{2}f^k{}_{mn}c^m{}_\pm c^n{}_\pm \tag{24}$$

where the L's are given by the following equations

$$L^+{}_kX^{p,q}=A^p{}_kX^{p-k,q}$$
$$L^-{}_kX^{p,q}=A^p{}_kX^{p,q-k} \tag{25}$$

where $A^p{}_q=k(k-1)\cdots(k-p+1)$. $f^k{}_{mn}=(m-n)\delta^k{}_{m+n}$ are the structure constants of the Virasoro algebra. In fact $L^\pm{}_k$ represent on $X^{p,q}$ two copies of the Virasoro algebra since their definition yields

$$[L^\pm{}_m,L^\pm{}_n]=f^k{}_{mn}L^\pm{}_k,\quad [L^+{}_m,L^-{}_n]=0 \tag{26}$$

In this new basis the operators

$$\Delta^\pm{}_0=(s,\frac{\partial}{\partial c^0{}_\pm}) \tag{27}$$

are diagonal on all X's and c's on which they have a very simple action

$$\Delta^+{}_0X^{p,q}=pX^{p,q}\quad \Delta^\pm{}_0c^n{}_\pm=nc^n{}_\pm$$
$$\Delta^-{}_0X^{p,q}=qX^{p,q}\quad \Delta^\pm{}_0c^n{}_\mp=0 \tag{28}$$

The eigenvalues of the pair $(\Delta^+{}_0,\Delta^-{}_0)$ on this basis is called *the total weight*. For instance $X^{p,q}$ have the total weight (p,q) while $c^n{}_+$, $c^n{}_-$ have the total weight (n,0) and (0,n) respectively.

The operators $\Delta^\pm{}_0$ are differentials, so the total weight of a monomial formed from the new basis is the sum of all total weights of the elements from the basis which enter in it. Let ω_0 be a monomial of total weight (p,q) with $pq\neq 0$ and $s\omega_0=0$. If $p\neq 0$ then we can write

$$p\omega_0=\Delta^+{}_0\omega_0=s[\frac{\partial}{\partial c^0{}_+}\omega_0] \tag{29}$$

or

$$\omega_0=s[\frac{1}{p}\frac{\partial}{\partial c^0{}_+}] \tag{30}$$

i.e., ω_0 is zero in the cohomology group.

Thus all solutions of the equation $s\omega_0=0$ which are not trivial *must have the total weight equal to (0,0).*

We can build up the solutions of the equation $s\omega_0=0$ in a smaller space generated by the new basis with the total weight (0,0). We have analyzed all monomials with the total weight (0,0) and we have found that for gh=0 there is only one such of monomial, for gh=1 there are 4, for gh=2 there are 9, for gh=3 there are 12, for gh=4 there are 9, for gh=5 there are 4 and finally for gh=6 there is one monomial. A detailed version of this analysis is given elsewhere [7]. Moreover, we have found out, in the space of these monomials, the solutions of the above equation which are not trivial. In fact we have obtained 10 independent and nontrivial solutions of the equation $s\omega_0=0$ with gh=2,3,4,5 and 6. The cohomology group $H^{*}(s)$ at ghost number greater than six vanishes in the space of local functionals.

4. RESULTS AND DISCUSSION. Now we are going to spell out our results for the solutions of the descent equations for all ghost numbers. Once we have all nontrivial elements of the cohomology group we have to integrate them and to obtain the solutions of the descent equations. We shall make use of an operator introduced in [1] denoted by δ and which can be written in our case as

$$\begin{aligned} \delta c^{+} &= dx^{+} h_{++} dx^{+} \\ \delta\phi &= 0 \end{aligned} \tag{31}$$

where $\phi=(X,h_{++})$ and it obeys the commutation relation

$$-[s,\delta]=d \tag{32}$$

With this operator at hand we deduce the following expressions of one-form respectively two-

form that appear in the descent equations:

$$\omega_1=\delta\omega_0 \quad \omega_2=\frac{1}{2}\delta^2\omega_0 \tag{33}$$

The complete results of our analysis can be summarized in the following discussion:

a) For gh=0 we have only one solution of the form

$$\omega_2=(1-y)X^{1,0}X^{0,1}Fdx^+\wedge dx^- \tag{34}$$

If we add the indices for $X=X^\mu$, $F=F_{\mu\nu}$ and take into consideration the form of $X^{1,0}, X^{0,1}$ we get eventually the classical action for the bosonic string

$$S_0=\int d^2x(\frac{1}{2}\sqrt{g}\,g^{\alpha\beta}G_{\mu\nu}\partial_\alpha X^\mu\partial_\beta X^\nu+B_{\mu\nu}(X)\partial_+X^\mu\partial_-X^\nu) \tag{35}$$

with $G_{\mu\nu}, B$ arbitrary functions of X satisfying

$$G_{\mu\nu}=G_{\nu\mu}, \quad B_{\mu\nu}=-B_{\nu\mu}$$

b) For gh=1 we have obtained four solutions of the descent equations which represent the coordinate anomalies. This integral forms can be written, after some partial integration, in the form

$$\begin{aligned}A=&\int d^2x[a_+c^+\partial^3_+h_{++}+a_-c^-\partial^3_-h_{--}\\&+\frac{1}{1-y}[(\partial_+\xi^+h_{--}\partial_-\xi^-)f^+_{\mu\nu}(X)+(\partial_-\xi^-h_{++}\partial_+\xi^+)f^-_{\mu\nu}(X)]\nabla^\mu_+X\nabla^\nu_-X]\end{aligned} \tag{36}$$

where a_+, a_- are constants $f^+_{\mu\nu}, f^-_{\mu\nu}$ are arbitrary functions of the matter fields and

$$\begin{aligned}\xi^\pm&=\frac{1}{1-y}(c^\pm-h_{\pm\pm}c^\mp)\\\nabla_\pm X&=(\partial_\pm-h_{\pm\pm}\partial_\mp)X\end{aligned} \tag{37}$$

c) For gh=2 we have got two independent solutions which have the following integral form

$$A^2=\int d^2x[\xi^1_+\xi^2_-\nabla_+X^\mu f^1_\mu(X)+\xi^1_-\xi^2_+\nabla_-X^\mu f^2_\mu(X)+\frac{1}{1-y}\xi^1_+\xi^1_-\nabla_+X^\mu\nabla_-X^\nu f_{\mu\nu}(X)] \tag{38}$$

where

$$\xi^1_{\pm} = \partial_{\pm}\xi^{\pm} + h_{\pm\pm}\partial_{\pm}\xi^{\pm} \qquad (39)$$
$$\xi^2_{\pm} = \partial^2_{\pm}\xi^{\pm} + 2(\partial_{\pm}h_{\pm\pm})(\partial_{\pm}\xi^{\pm})$$

and $f^{1,2}{}_{\mu}(X)$, $f_{\mu\nu}(X)$ are some arbitrary functions of X

d) **For gh=3** we have also obtained two independent solutions with the integral given by

$$A^3 = \int d^2x[\xi^1_{+}\xi^1_{-}\xi^2_{+}\nu_{-}X^{\mu}f^1{}_{\mu}(X) + \xi^1_{+}\xi^1_{-}\xi^2_{-}\nu_{+}X^{\mu}f^2{}_{\mu}(X)] \qquad (40)$$

e) **For gh=4** we give the last solution of the descent equations. It has the following form

$$A^4 = \int d^2x(1-y)\xi^1_{+}\xi^1_{-}\xi^2_{+}\xi^2_{-}F(X) \qquad (41)$$

with $F(X)$ an arbitrary scalar function of X.

5. CONCLUSIONS. In this paper we have given all nontrivial local solutions of the equation $s\omega_0=0$, i.e., all members of the BRST cohomology group and all members of it in the space of *local functionals*, i.e., all solutions of the descent equations for the 2D conformal gravity. It is remarkable to point out that this case is the unique case in literature, to our knowledge, except the Yang-Mills case where all the problem reduces to the cohomology of the Lie algebra, where all the BRST cohomology has been calculated.

The same method have been applied by the present authors for other models [7] and the results will be published elsewhere.

REFERENCES

1. S.P. Sorella Comm. Math. Phys. 157(1993),231;S.P. Sorella and L. Tataru, Phys. Lett. B324(1994), 351;
2. C. Becchi, A. Rouet and R. Stora, Ann. Phys.(N.Y.) 98,(1976) 287; I.W. Tyutin, Gauge Invariance in Field Theory and Statistical Physics, Lebedev Institute preprint FIAN no., 39(1975);
3. I.A. Batalin and G.A. Vilkovisky, Phys. Rev. D28 (1983) 2567;
4. M.Henneaux and C. Teitelboim, Quantization of Gauge Systems, Princeton University Press, 1992;G Barnich, F. Brandt and M. Henneaux, preprint ULB-TH-94/06, NIKEF-H 94-13, hep/th/940510916.A Boresch, M. Schweda and S.P. Sorella, Phys. Lett. B328(1994);

5. R. Utiyama, Phys. Rev., 101, (1956) 1597;
6. E. Witten, Comm. Math. Phys., 117(1988) 353; Comm. Math. Phys. 118(1988) 411;
7. P. A. Blaga, L.Tataru, I. V. Vancea, BRST cohomology for 2D gravity, to be published.
8. C. Becchi, Nucl. Phys. B304 513;
9. L. Baulieu, C. Becchi and R. Stora, Phys. Lett. B180(1986), 55; KUL-TF-94/94, hep-th/9410162.
10. L. Baulieu and M. Bellon, Phys. Lett. B196(1987), 142; R. Grimm, Ann. Phys.(N.Y.) 200(1990) 49;
11. R. Stora, Algebraic structure and topological origin of anomalies, Cargese '83, G. t'Hooft et al., Plenum Press, New York, 1987;
12. J. Dixon, Comm. Math. Phys., 139(1991) 495;
13. M. Werneck de Oliveira, M. Schweda and S.P. Sorella, Phys. Lett. B315(1993) 93;
14. F. Brandt, W. Troost and A. Van Proeyen ,NIKHEF-H 94-16, KUL-TF-94/17, hep-th/9407061, to appear in the proceedings of the Geometry of Constrained Dynamical Systems workshop, Isaac Newton Institute for Mathematical Sciences, Cambridge, June 15-18, 1994.
15. F. Brandt, N. Dragon and M. Kreuzer, Nucl. Phys B340(1990) 187;

STUDIA UNIV. BABEŞ-BOLYAI, PHYSICA, XXXIX, 1, 1994

HYDROMAGNETIC CONVECTIVE FLOW THROUGH A HORIZONTAL CHANNEL IN THE PRESENCE OF HALL EFFECT

A. MARCU and M. VASIU*

Received: 20.12.1993

ABSTRACT. - The Hall effect on hydromagnetic free and forced convection flow of an electrically conducting fluid, through an horizontal channel with porous walls permeated by a uniform transverse magnetic field , has been considered. Considering the wall temperature to vary linearly with distance, and the suction parameter zero, we have been obtained the solution for velocity and induced magnetic field. This paper is an response to the mistake in non-dimensional quantities used in [3].

I. INTRODUCTION. The problem of free convective flow of an electrically conducting fluid, permeated by uniform magnetic field, assuming the axial temperature variation along the wall have been studied by many authors [1], [2] Such studies are of a great importance in the magnetohydrodynamic generators design, in the cooling of nuclear reactor etc.

The purpose of this paper is to consider the problem of Hall effect in free and forced convection flow of a conducting fluid through an horizontal channel, the walls beeing porous and the suction parameter zero. The behavior of the velocity and the magnetic field are shown graphically.

II. FORMULATION OF THE PROBLEM. We suppose that an electrically conducting fluid flows between two horizontal porous walls at the distance 2l apart. We shell

* *"Babeş-Bolyai" University, Faculty of Physics, 3400 Cluj-Napoca, Romania*

assume that the x and y axes are along and perpendicular to the walls with the origin midway between them The fluid is permeated by an uniform magnetic field B_0 applied paralel to the y-axis and dp/dx is constant [3]

For steady motion of a viscous, incompressible and conducting fluid all phisical quantities except temperature and pressure are functions of y alone [4]. The equations for motion, magnetic induction, energy and continuity are:

$$\rho(\vec{v}\nabla)\vec{v}=-\nabla p+\vec{j}\times\vec{B}+\eta\nabla^2\vec{v}+\rho\vec{g} \qquad (1)$$

$$\nu_m\nabla^2\vec{B}+\nabla\times(\vec{v}\times\vec{B})-\frac{\beta}{\mu}\nabla\times[(\nabla\times\vec{B})\times\vec{B}]=0 \quad (2)$$

$$\vec{j}=\sigma[\vec{E}+(\vec{v}\times\vec{B})-\beta(\vec{j}\times\vec{B})] \qquad (3)$$

$$(\vec{v}\nabla)\theta=\alpha\nabla^2\theta+\phi+\frac{j^2}{\sigma} \qquad (4)$$

$$\nabla\cdot\vec{v}=0 \qquad (5)$$

where ρ is the density, $\vec{v}$ the velocity, $\vec{B}$ the induced magnetic field, p the pressure, μ magnetic permeability, η the kinematic viscosity, ν_m the magnetic viscosity, β the Hall const., θ the temperature, α the thermal difusivity, Φ the viscous dissipation function, $\vec{J}$ the curent density and σ the electrical conductivity.

Neglecting the suction parameter we take the velocity, magnetic field, and the curent intensity as:

$$\vec{v}=[u(y),0,w(y)];$$
$$\vec{B}=[b_x(y),B_0,b_z(y)];$$
$$\vec{j}=[j_x(y),0,j_z(y)];$$

The governing equation of motion are: $[0,\theta,-g]$;

$$\frac{\partial p}{\partial x}=-j_z B_o+\eta\frac{d^2u}{dy^2} \tag{6}$$

$$\frac{\partial p}{\partial y}=(j_z b_x-j_x b_z)-\rho g \tag{7}$$

$$0=j_x B_o+\eta\frac{d^2w}{dy^2} \tag{8}$$

Taking in account (2) and (3) we get:

$$\frac{db_z}{dy}=\mu j_x; j_x=\sigma[E_x-wB_o+\beta j_z B_o] \tag{9}$$

$$\frac{db_x}{dz}-\frac{db_z}{dx}=0; j_y=\sigma[wb_x-ub_z-\beta(j_z b_x-j_x b_z)]=0 \tag{10}$$

$$-\frac{db_x}{dy}=\mu j_z; j_z=\sigma[E_z+uB_o-\beta j_x B_o] \tag{11}$$

From (11) and (6)

$$\frac{\partial p}{\partial x}=\frac{B_o}{\mu}\frac{db_x}{dy}+\eta\frac{d^2u}{dy^2}=0 \tag{12}$$

introducing (11) in (9) we get:

$$j_x=\sigma[E_x-wB_o-\frac{\beta B_o}{\mu}\frac{db_x}{dy}] \tag{13}$$

The equations (9) and (11) together yield:

$$\frac{B_o}{\mu}\frac{db_z}{dy}+\eta\frac{d^2w}{dy^2}=0 \tag{14}$$

$$j_x=\sigma[E_x+uB_0-\frac{\beta B_0}{\mu}\frac{db_z}{dy}] \tag{15}$$

we get from (10) for ($\sigma = 0$):

$$b_x(w-\beta j_z)=b_z(u-j_x\beta) \tag{16}$$

and adding eq (7) we obtain:

$$\frac{\partial p}{\partial y}=b_x[(1+\beta)j_z-w]-b_z[(1+\beta)j_x-u]-\rho g \tag{17}$$

Introducing (11) and (9) in (17) results:

$$\frac{\partial p}{\partial y}=-(\frac{1+\beta}{2\mu})\frac{d}{dy}(b_x^2+b_z^2)-wb_x+ub_z-\rho g \tag{18}$$

Equation (11) with (13) yield

$$\frac{d^2b_z}{dy^2}+\omega\tau\frac{d^2b_x}{dy^2}+\mu\sigma B_o\frac{dw}{dy}=0 \tag{19}$$

$$\beta=\frac{\omega\tau}{}$$

where ω is the electron Larmor frequency and τ the mean interval between the succesive collision of an electron with ions .

In this paper we have neglected the slip effects between ions and neutral particules and also the electron pressure gradient

Introducing (11) in (15) we get:

$$-\frac{d^2b_x}{dy^2}+\omega\tau\frac{d^2b_z}{dy^2}-\mu\sigma B_o\frac{du}{dy}=0 \tag{20}$$

The governing equation of motion and for magnetic field are:

$$\frac{\partial p}{\partial x}=\frac{B_o}{\mu}\frac{db_x}{dy}+\eta\frac{d^2u}{dy^2} \tag{21}$$

$$\frac{\partial p}{\partial y}=-(\frac{1+\beta}{2\mu})\frac{d}{y}(b_x^2+b_z^2)-wb_x+ub_z-\rho g \tag{22}$$

$$0=\frac{B_o}{\mu}\frac{db_x}{dy}+\eta\frac{d^2w}{dy^2} \tag{23}$$

$$\frac{d^2b_z}{dy^2}+\omega\tau\frac{d^2b_x}{dy^2}+\mu\sigma B_o\frac{dw}{dy}=0 \tag{24}$$

$$\omega\tau\frac{d^2b_z}{dy^2}-\frac{d^2b_x}{dy^2}-\mu\sigma B_o\frac{du}{dy}=0 \tag{25}$$

We assume a linar uniform temperature variation along the lower wall y=1 in the form

$$T=T_o+kx+P(y)\,;\quad k=const \tag{26}$$

Equation of state becomes:

$$\rho = \rho_o - \rho_o \alpha k x - \rho_o \alpha F(y) \tag{27}$$

Taking account of (10), eq.(22) becomes:

$$\frac{dp}{dy} = -\frac{1}{2\mu}\frac{d}{dy}(b_x^2 + b_z^2) - \rho g \tag{28}$$

Equations (28) and (27) by integration yield:

$$P = -\frac{1}{2\mu}(b_x^2 + b_z^2) - \rho_o g y - \rho_o g \alpha k x y - \rho_o g \alpha \int F(y)dy + f(x) \tag{29}$$

We have introduced the folowing non-dimenional quantities:

$$y^* = \frac{y}{l}; \quad u^* = \frac{ul}{\nu\Delta}; \quad \Delta = \frac{\partial p}{\partial x} = \frac{l^3}{\partial \rho_0 \nu^2}\frac{df(x)}{dx},$$

$$b_x^* = \frac{b_x}{\mu\sigma B_0 \nu\Delta}; \quad b_z^* = \frac{b_z}{\mu\sigma B_0 \nu\Delta}; \quad P_m = \mu\sigma\nu; \tag{30}$$

$$H_a^2 = \frac{B_0 l^2 \sigma}{\rho_0 \nu}; \quad O = \frac{g\alpha k l^4}{\nu^2 \Delta}$$

From (29) result:

$$\frac{\partial p}{\partial x} = -\rho_o g \alpha k y + \frac{df(x)}{dx}$$

and together with (21) yield:

$$\eta\frac{d^2u}{dy^2} + \frac{B_o}{\nu}\frac{db_x}{dy} + \rho_o g \alpha k y = \frac{df(x)}{dx}$$

Taking in account (30) and (23) we obtain:

$$\frac{d^2u^*}{dy^{*2}} + H_a^2\frac{db_x^*}{dy^*} + Oy^* = 1 \tag{31}$$

$$\frac{d^2w^*}{dy^{*2}} + H_a^2 \frac{db_z^*}{dy^*} = 0 \tag{32}$$

Considering $V=u^*+iw^*$; $b=b^*_x+ib^*_z$, from (31) and (32) result:

$$\frac{d^2V}{dy^{*2}} + H_a^2 \frac{db}{dy^*} + Oy^* = 1 \tag{33}$$

From (24) and (25) with (30)

$$\frac{d^2b_z^*}{dy^{*2}} + \omega\tau \frac{d^2b_x^*}{dy^{*2}} + \frac{dw^*}{dy^*} = 0 \tag{34}$$

$$\omega\tau \frac{d^2b_z^*}{dy^{*2}} - \frac{d^2b_x^*}{dy^{*2}} - \frac{du^*}{dy^*} = 0 \tag{35}$$

and considering (33) we get:

$$\frac{d^2b}{dy^{*2}} = -\frac{1}{1+i\omega\tau} \frac{dV}{dy^*} \tag{36}$$

Integrating (36) we get

$$\frac{db}{dy^*} = k_1 - \frac{1}{1+i\omega\tau} V; \quad k_1 = const. \tag{37}$$

and together with (33) yield:

$$\frac{d^2V}{dy^{*2}} - k_2^2 V - f(y^*) = 0 ;$$

$$f(y^*) = R + Oy^* ; \; R = H_a^2 k_1 - 1 ; \; k_2^2 = \frac{H_a^2}{1+i\omega\tau} ; \tag{38}$$

$$\frac{db}{dy^*} = k_1 - \frac{k_2^2}{H_a^2} V , \tag{39}$$

The boundary conditions [5] are:

$$y^* = 1 \; ; \; V = V_1 \; ; \; \sigma_1 \frac{db}{dy^*} + b = 0$$
$$y^* = -1 \; ; \; V = V_2 \; ; \; \sigma_2 \frac{db}{dy^*} - b = 0 \qquad (40)$$

where σ_1, σ_2 are the electric conductance ratio of the walls.

Taking into account (38)-(39) and (40) we obtain:

$$\sigma_1 \cdot (k_1 - \frac{k_2^2}{H_a^2} V_1) + b = 0 \quad ; \quad \sigma_2 \cdot (k_1 - \frac{k_2^2}{H_a^2} V_2) - b = 0 \qquad (41)$$

and

$$k_1 = \frac{k_2^2}{H_a^2} \cdot \frac{\sigma_1 V_1 + \sigma_2 V_2}{\sigma_1 + \sigma_2} \qquad (42)$$

$$b = \frac{1}{2} \cdot [k_1 (\sigma_2 - \sigma_1) + \frac{k_2^2}{H_a^2} \cdot (\sigma_1 V_1 + \sigma_2 V_2)] \qquad (43)$$

$$\Rightarrow \quad b = \frac{k_2^2}{H_a^2} \cdot \frac{\sigma_1 \sigma_2}{\sigma_1 + \sigma_2} \cdot (V_1 - V_2) \qquad (44)$$

III. SOLUTIONS OF THE PROBLEM. The solution of the (38) is:

$$V = C_{10} \cdot chk_2 y^* + C_{20} \cdot shk_2 y^* - \frac{2R}{k_2^2} \cdot shk_2 y^* \cdot shk_2$$

where (45)

$$C_{10} = \frac{V_1 + V_2}{2chk_2} \; ; \; C_{20} = \frac{V_1 - V_2}{2shk_2} + \frac{2R}{k_2^2} shk_2$$

Considering $\omega\tau = 1$, $V_1 = 1$ and $V_2 = 0$ we obtain:

$$u^* = \frac{1}{2} chay^* \cdot cha \cdot cosby^* \cdot cosb \cdot [\frac{1 + thay^* \cdot tha \cdot tgby^* \cdot tgb}{ch^2 a - \sin^2 b} + \frac{thay^* \cdot tha + tgby^* \cdot tgb}{sh^2 a + \sin^2 b}] \qquad (46)$$

$$w^* = \frac{1}{2}\cdot chay^*\cdot cha\cdot cosby^*\cdot cosb\cdot\left[\frac{thay^*\cdot tgby^* - tha\cdot tgb}{ch^2a - \sin^2 b} + \frac{tha\cdot tgby^* - thay^*\cdot tgb}{ch^2a + \sin^2 b}\right] \tag{47}$$

where

$$b_{1,2} = +\frac{H_a}{2}\cdot\frac{1}{\sqrt{1+\sqrt{2}}} \qquad a_{1,2} = \pm\frac{H_a}{2}\cdot\sqrt{1+\sqrt{2}} \qquad k_{2(1,2)} = \pm\frac{H_a}{2\sqrt{1+\sqrt{2}}}\cdot(1+\sqrt{2}-1)$$

The graphically results for velocity field distribution in the case of Ha = 5, 10 are presentated in figure 1-4

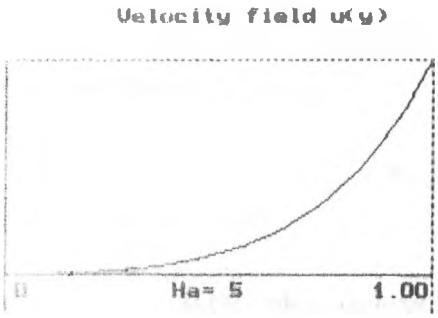

Figure 1

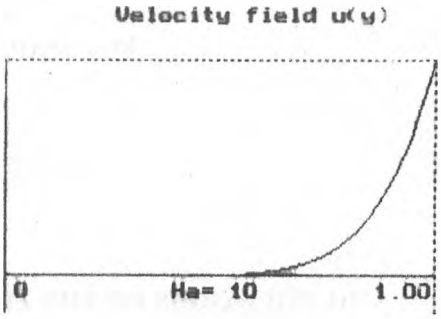

Figure 2

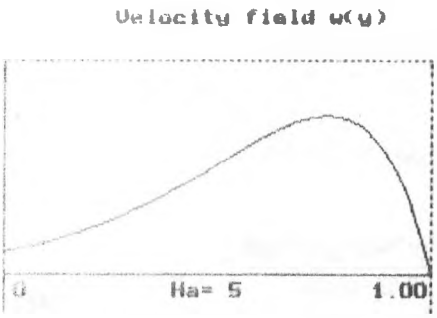

Figure 3

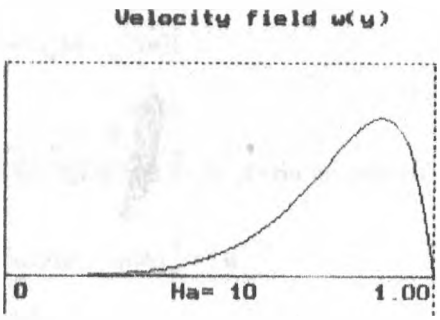

Figure 4

The decreasing values for velocity field with the increasing of induced magnetic field is clear for large value of Ha number but the behavior of velocity becomes arbitrary for small values of Ha number, these will be the subject of an other paper

REFERENCES

1 Grief R., Habib I.S., Lin J.C.: Fluid Mech 46 (1971) 513
2 Yu C.P.: AIAA 3(1965) 1184
3 Sanyal D.C., Samanta S.K.: Acta phys slov 38 (1988) 358.
4 Gupta A.S.: Appl. Sci. Res 9 (1960) 319
5. Cowling T.G.: Magnetohydrodynamics Adam Hilger 1976.

STUDIA UNIV. BABEŞ-BOLYAI, PHYSICA, XXXIX, 1, 1994

SUR UN MODELE MAGNETOHIDRODINAMIQUE D'UN PLASMA COSMIQUE COMPOSE EN MOUVEMENT DE ROTATION SOUS L'ACTION DE SON PROPRE CHAMP GRAVIFIQUE

M. [illegible]*

Received: 1.12.1993

ABSTRACT. - In the present paper we shall examine the magneto-gravitational stability of a composite rotating plasma. The plasma consists of an ionized component and a neutral component in uniform rotational motion with angular velocity Ω_i, Ω_n respectively. The ionized component is compressible, nonviscous, with finite resistivity , it is under the influence of a uniform vertical magnetic field. The neutral component is compressible and nonviscous. At the same time the plasma is assumed to be found under the influence of a proper gravitational field.

Introduction. Dans le present article nous voulons déduire l'équation de dispersion et le critère de stabilité magnéto- gravitationelle d'un modèle de plasma cosmique. Le plasma est constitué d'un composant ionique, compressible, nonvisqueux, doué d'une conductivité électrique finie, en mouvement de rotation uniforme avec une vitesse angulaire Ω_i $(0,0,\Omega_i)$ et d'un composant neutre, compressible, nonvisqueux, en mouvement de rotation avec une vitese angulaire Ω_n $(0,0,\Omega_n)$ $(\Omega_i = \Omega_n)$. Ce problème est analysé pour la première fois en littérature de spécialité. Le composant ionique et le composant neutre se trouvent sous l'action du même champ gravifique. En même temps le composant ionique est soumis sous l'action d'un champ magnétique uniforme $B_0(B_0,0,0)$. Nous utilisons les résultats obtenus par Bhatia [1], Hans [2], Mattei [3], Herrnegger [4], Vasiu [5],[6], Chandrasekhar [7] et en même temps nous généralisons ces résultats pour le modèle adopté.

* *"Babeş-Bolyai" University, Faculty of Physics, 3400 Cluj-Napoca, Romania*

Equations fondamentales pour l'état perturbé du plasma. Le système d'equations magnétohydrodynamiques por l'état perturbé du plasma s'écrit de la manière suivante:

$$\frac{\partial \vec{u}_i}{\partial t} = -\frac{1}{\rho_{io}}\nabla(\delta p_i)-\nabla(\delta V)+2\vec{u}_i\times\Omega_i+\nu_c(\vec{u}_n-\vec{u}_i) + \frac{1}{\mu_o\rho_{io}}(\nabla\times\delta B)\times B_o, \tag{1}$$

$$\frac{\partial \vec{u}_n}{\partial t} = -\frac{1}{\rho_{no}}\nabla(\delta p_n)-\nabla(\delta V)+2\vec{u}_n\times\Omega_n+\beta\nu_c(\vec{u}_i-\vec{u}_n), \tag{2}$$

$$\frac{\partial(\delta\rho_i)}{\partial t} = -\rho_{io}\nabla\cdot\vec{u}_i, \tag{3}$$

$$\frac{\partial(\delta\rho_n)}{\partial t} = -\rho_{no}\nabla\cdot\vec{u}_{no}, \tag{4}$$

$$\frac{\partial(\delta B)}{\partial t} = \nabla\times(\vec{u}_i\times B_o) + \nu_m\Delta(\delta B), \tag{5}$$

$$\Delta(\delta V) = K(\delta\rho_i + \delta\rho_n), \tag{6}$$

$$\delta p_i = V_{si}^2\delta\rho_i, \tag{7}$$

$$\delta p_n = V_{sn}^2\delta\rho_n, \tag{8}$$

où u_i, u_n, δB, δp_i, δp_n, $\delta\rho_i$, $\delta\rho_n$, δV sont les perturbations pour: la vitesse, le champ magnétique, la pression, la densité, le potentiel gravifique du plasma; V_{si}, V_{sn} sont les vitesses du son dans le composant ionique respectivement dans le composant neutre,

ν_c est la fréquence des collisions entre les ions et les atomes; $\beta=\rho_{io}/\rho_{no}$,ν_m est le coefficient de viscosité magnétique du plasma; K est la constante gravitationelle

les indice i, n marquent le composant ionique et respectivement le composant neutre

Admettons que des petites perturbations $\delta\varphi(z,t)$ se propagent dans le plasma sous la forme

$$\delta\varphi(z,t) = \varphi^{*}\exp[i(kz-\omega t)] \tag{9}$$

où φ^{*} est l'amplitude, k est le nombre d'onde, ω est la pulsation de la perturbation, t est le temps

Admetons que les petites perturbations se propagent le long de l'axe Oz

Introduisant les vecteurs de déplacement infinitésimal $\xi_{si}(\xi_{six},\xi_{siy},\xi_{siz})$ et $\xi_{sn}(\xi_{snx},\xi_{sny},\xi_{snz})$ pour les composants du plasma

$\vec{u}_i = \dfrac{\partial\vec{\xi}_{si}}{\partial t} = -i\omega\vec{\xi}_{si}$, $\vec{u}_n = \dfrac{\partial\vec{\xi}_{sn}}{\partial t} = -i\omega\vec{\xi}_{sn}$, et aussi les constantes

$$A = \omega^2 + i\omega\nu_c \; ; \; B = -2i\omega\Omega_i \; ; \; C = \omega^2 + i\omega\nu_c + K\rho_{no} - k^2V_{ni}^2 + \frac{i\omega k^2V_A^2}{\Omega_m} \; ,$$

$$D = -2i\omega\Omega_m \; ; \; E = -(i\omega\nu_c - K\rho_{no}\rho) \; ; \; F = -i\omega\beta\nu_c \; , \; G = \omega^2 + i\omega\beta\nu_c \; ; \tag{10}$$

$$H = -2i\omega\Omega_n \; ; \; I = -(i\omega\beta\nu_c - K\rho_{no}) \; ; \; J = \omega^2 + i\omega\beta\nu_c - k^2V_{nn}^2 + K\rho_{no}\rho \; ,$$

où $V_A^2 = \dfrac{B_o^2}{\mu_o\rho_{no}}$ est la vitesse Alfvén, $\Omega_m = -i\omega + \nu_m k^2$, $\rho = \dfrac{\rho_{no}}{\rho_{io}} = \dfrac{1}{\beta}$,

faisant les calculs, en tenant compte des équations (3)-(6) et des relations (7)-(8), les équations (1)-(2), en projections sur les axes Ox, Oy, Oz, s'écrivent sous la forme

$$A\xi_{sx} + B\xi_{sy} + D\xi_{nx} = 0 \tag{11}$$

$$-B\xi_{sx} + A\xi_{sy} + D\xi_{ny} = 0 \tag{12}$$

$$C\xi_{sz} + F\xi_{nz} = 0 \tag{13}$$

$$F\xi_{sx} + G\xi_{nx} + H\xi_{ny} = 0 \tag{14}$$

$$F\xi_{sy} + G\xi_{ny} - H\xi_{nx} = 0 \tag{15}$$

$$I\xi_{sz} + J\xi_{nz} = 0 \tag{16}$$

Équation de dispersion L'équation de dispersion s'obtient par l'annulation du déterminant formé par les coefficients des grandeurs ξ_{sx}, ξ_{sy}, ξ_{sz}, ξ_{nx}, ξ_{ny}, ξ_{nz}

$$\begin{vmatrix} A & B & 0 & D & 0 & 0 \\ -B & a & 0 & 0 & D & 0 \\ 0 & 0 & C & 0 & 0 & F \\ F & 0 & 0 & G & H & 0 \\ 0 & F & 0 & 0 & G & -H \\ 0 & 0 & I & 0 & 0 & J \end{vmatrix} = 0 \tag{17}$$

Faisant les calculs on obtient les équations de dispersion

$$CJ - IE = 0 \tag{18}$$

$$G^2(A^2+B^2)-2ADFG+BD^2FH = 0 \tag{19}$$

Limitons maintenant l'annalyse seulement pour l'équation (18), qui, en tenant compte de (10), s'écrit sous la forme

$$[\sigma^2 + \sigma(\nu_c + \frac{k^2V_A^2}{\sigma + \nu_m k^2} + \Omega_{jn}^2](\sigma^2 + \sigma\beta\nu_c + \Omega_{jn}^2] - \\ -(\sigma\beta\nu_c + K\rho_{io})(\sigma\nu_c + K\rho_{io}\rho) = 0 , \tag{20}$$

où $\Omega_{jn}^2=k^2V_n^2-K\rho_{io}$, $\Omega_{jn}^2=k^2V_{sn}^2-K\rho_{no}$, $\sigma=i\omega$

Cas particulier Supposant que les collisions entre les ions et les atomes et aussi la conductivité electrique du plasma sont négligeables ($\nu_c=0$, $\nu_m=0$), l'équation (20) prend la forme

$$\sigma^4 + b_1\sigma^2 + b_2 = 0 \tag{21}$$

$$b_1 = k^2(V_n^2 + V_{sn}^2 + V_A^2) - K(\rho_{io} + \rho_{no}) \tag{22}$$

$$b_2 = \Omega_{jn}^2\Omega_{jn}^2 + k^2V_A^2\Omega_{jn}^2 - K^2\rho_{no}\rho_{no}$$

Dans ce cas particulier le mouvement de rotation ne joue pas aucun rôle sur la stabilité magnetogravitationelle du système. Introduisant les notations utilisées par Hermegger [4], mais adaptées pour le modèle analysé

$$\hat{a} = \frac{V_{sn}}{V_{si}} , \; A = \frac{V_A}{V_{si}} , \; \rho = \frac{\rho_{no}}{\rho_{io}} \tag{23}$$

$$\overline{k} = \frac{kV_{si}}{\sqrt{K\rho_{io}}} , \; \overline{\sigma} = \frac{\sigma}{\sqrt{K\rho_{io}}} , \tag{24}$$

l'équation (21) s'écrit de la manière suivante

$$\overline{\sigma}^4 + b_1\overline{\sigma}^2 + b_2 = 0 , \tag{25}$$

où

$$b_1 = \overline{k}^2(1 + \hat{a}^2 + A^2) - (1 + \rho) ,$$
$$b_2 = \overline{k}^2[(\hat{a}^2\overline{k}^2 - \rho)(1 + A^2) - \hat{a}^2] \tag{26}$$

l'équation (25) est identique avec l'équation obtenue par Hermegger, mais en l'absence de "Finite Larmor Radius" (la gyroviscosité $\nu = 0$)

Prenant en considération l'équation (25) il en résulte que nous pouvons écrire, pour $b_2 < 0$, l'inégalité

$$\overline{\sigma}_1^2\overline{\sigma}_2^2 = b_2 = \overline{k}^2[\hat{a}^2\overline{k}^2 - \rho)(1 + A^2) - \hat{a}^2] < 0 , \tag{27}$$

de sorte que $\overline{\sigma}_1^2 < 0$ *et* $\overline{\sigma}_2^2 > 0$, *ou* $\overline{\sigma}_2^2 < 0$ *et* $\overline{\sigma}_1^2 > 0$

Introduisant maintenent la fonction $F(\overline{k})$

$$F(\overline{k}) = \overline{k}^2[(\hat{a}^2\overline{k}^2 - \rho)(1 + A^2) - \hat{a}^2] \tag{28}$$

Si nous considerons $F(\overline{k}) = 0$ on peut déterminer la valeur critique k_c du nombred'onde $\overline{k}$

Faisant les calcules on obtient

$$k_c = \frac{k}{\bar{k}}\left[\frac{\rho(1+A^2) + \hat{a}^2}{\hat{a}^2(1 + A^2)}\right]^{\frac{1}{2}}, \qquad (29)$$

$$où \ \frac{k}{\bar{k}} = \frac{\sqrt{K\rho_\omega}}{V_{si}}$$

Si les perturbations ont le nombre d'onde $k > k_c$ le système est **stable**, au contraire si $k < k_c$ le système est **instable**, sous l'aspect magnéto-gravitationnelle

Les graphiques de la fonction $F(\bar{k})$ pour les valeurs: A=5, ρ=10, â=1, A=10, ρ=10, â=1, A=50, ρ=10, â=1; $\bar{k}$ =[0,4] est présenté dans les figures 1-3

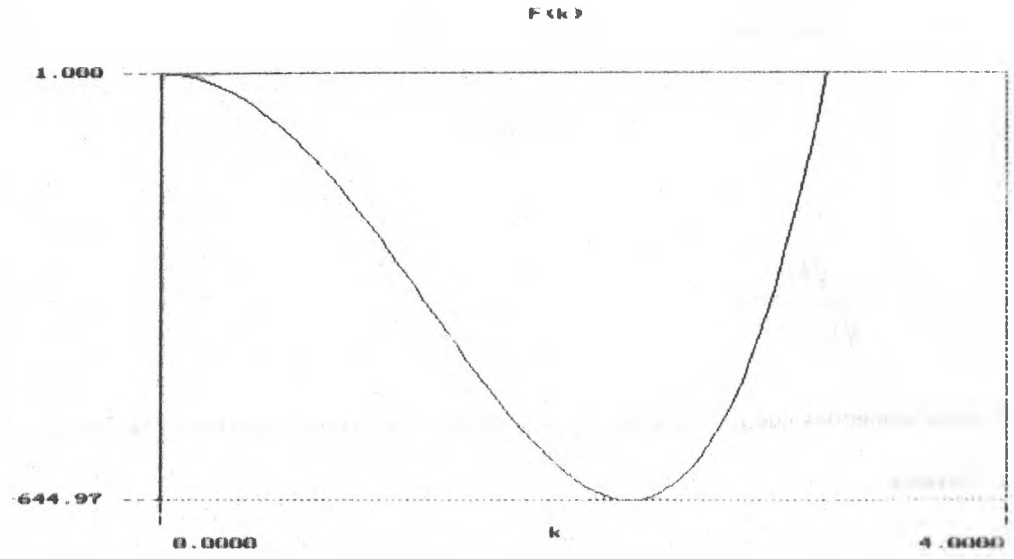

Figure 1

Pour le cas d'un modèle de plasma constitué par un seul composant ionisé, donc ρ=0, la formule (29) prend la forme

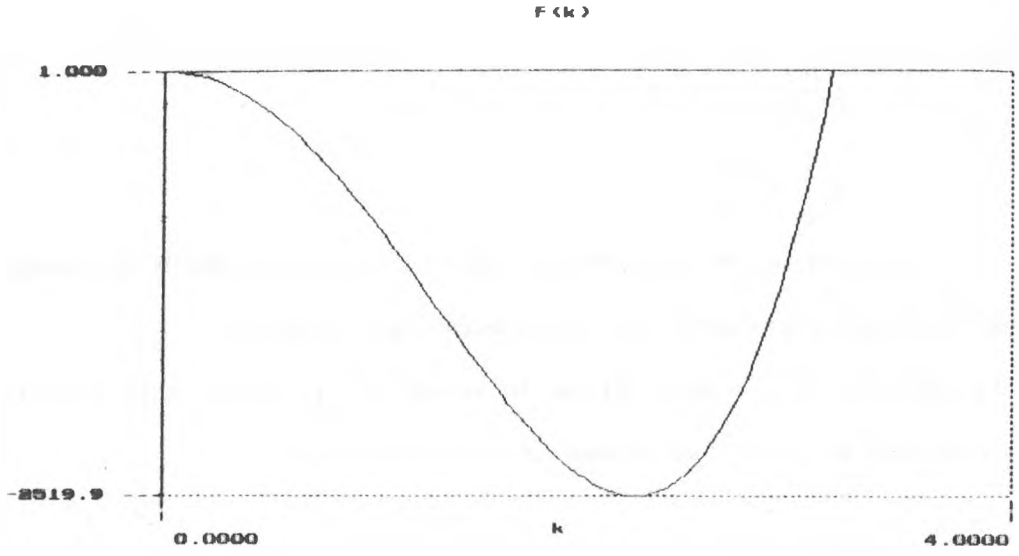

Figure 2

$$k_c = \frac{\sqrt{K\rho_{i0}}}{\sqrt{V_{si}^2 + V_a^2}} \tag{30}$$

Si nous admettons que ρ=0 et aussi V_A=0 (l'absence du champ magnetique) la formule (29) se réduit à

$$k_c = k_J = \frac{\sqrt{K\rho_{i0}}}{V_{si}} \tag{31}$$

qui est le nombre d'onde établi par Jeans [7]

Figure 3

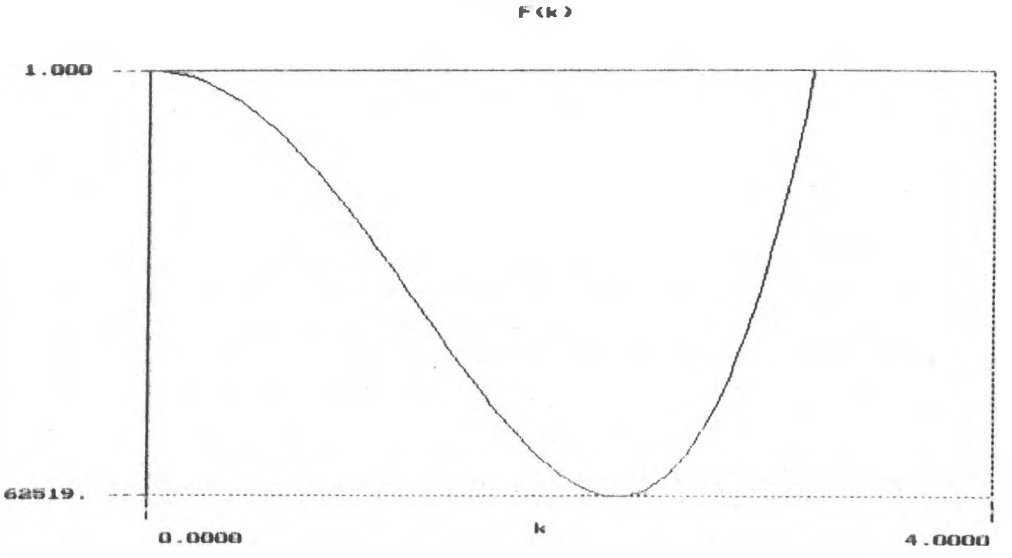

BIBLIOGRAPHIE

1 P Bhatia, Astron a Astrophys , 1, 399(1969)
2 H. Hans, Nucl Fusion, 10, 89(1968)
3 G Mattei, J. Plasma Phys., 2, 9(1968)
4 F Hermegger, J. Plasma Phys , 8, 393(1972)
5 M Vasiu, Studia Univ. Babes-Bolyai, Physica, 1, 54(1979)
6 M Vasiu, Conférence Nat de Gravité et Rélativité Générale, Bistrita, Roumanie, mai 1993 (sera publié)
7 S Chandrasekhar, Hydrodynamic and Hydromagnetic Stability, Clarendon Press, Oxford.chap XIII, 120

STUDIA UNIV. BABEŞ-BOLYAI, PHYSICA, XXXIX, 1, 1994

ON THE APPLICABILITY OF THE QUANTUM MONTE CARLO METHOD

Z. NÉDA*, R. ALBERT*, I. ALBERT*, T. NÉDA*

Received: 20.06.1994

ABSTRACT. - Considering the analitically well-understood problem of one quantum particle in an infinite deep potential valley and in thermal contact with a heat-bath, we comment on the applicability of quantum Monte Carlo methods. We study sistematicly the influence of different parameters on the relative error of the method and a phenomenological criteria for the maximal relative error is established.

1. Introduction. Lattice models proved to be a useful tool in studying many-body systems. We mention in this sense problems related with strongly correlated electron systems [1,2], degenerate electron gas in the periodic potential of a lattice [3], quantum-spins [4,5] and quantum-chromodinamical (QCD) systems [6].

Discretizing the space and considering the hamiltonian in a second quantized formalism, it is possible to study quantum-statistical systems in analogy with the well-known Ising model. The computer simulation method considered for discretized quantum-statistical problems in canonical ensambleis known in the literature [7-11] as the Quantum Monte Carlo (QMC) method.

The aim of our paper is to discuss on the aplicability of this method. In this sense we consider the simple well-studied problem of one particle in an infinite deep potential valley in thermal contact with a heat-bath, and compare our simulation results with the exact analitical ones. For simplicity, we will focus on the one-dimensional case.

* *"Babeş-Bolyai" University, Faculty of Physics, 3400 Cluj-Napoca, Romania*

Our work is justified by the importance of the QMC method in many-body physics, by the hopes that computational results could improve the understanding of exactly non-solvable quantum-statistical models, and by the great importance of the tractable problems. This study is only a first step, and for further investigations we will consider some exactly non-solvable problems, which are presented in the next section. For performing the proposed studies on the practically important models we must have a level of confidence in the results ofered by the QMC method. Our paper is intended to give contributions in these sense, testing the program elaborated by us and the computational resources necessary for achieving the equilibrium values of the interesting physical quantities. We are also interested in finite-size effects, in the errors introduced by the space discretization and by the used Trotter-Suzuki [12] approximation.

We will try to present the problem in a pedagogical manner, emphasizing also on the effective realization of the QMC simulations.

2. Lattice models for quantum-statistical problems

2.1. Quantum spin models. In the study of magnetic ordering we are faced with quantum mechanical problems on discretized lattices. The most known among these is the quantum spin model [4,5], widely used to describe the magnetic ordering in insulators. The hamiltonian of the model is:

$$\hat{H}=-J_{xy}\cdot\sum_{i,j}[\hat{S}_j^x\cdot\hat{S}_i^x+\hat{S}_j^y\cdot\hat{S}_i^y]-J_z\cdot\sum_{i,j}\hat{S}_j^z\cdot\hat{S}_i^z \qquad (1)$$

with S^α the components of the spins, and the sum refering usually just to nearest spin neighbours. As special cases of the quantum spin model we have:

- for $J_{xy}=J_z$ the Heisenberg model

- for $J_{xy}=0$ the Ising model

- for $J_z=0$ the XY model

By using the well-known "raising" $\hat{S}^+=\hat{S}^x+i\hat{S}^y$ and "lowering" $\hat{S}^-=\hat{S}^x-i\hat{S}^y$ operators the hamiltonian of the system can be written in a similar form with a second quantized hamiltonian:

$$\hat{H}=-\frac{J_{xy}}{2}\cdot\sum_{i,j}\left[\hat{S}_i^+\cdot\hat{S}_i^-+\hat{S}_i^+\cdot\hat{S}_j^-\right]-J_z\cdot\sum_{i,j}\hat{S}_j^z\cdot\hat{S}_i^z \tag{2}$$

In a one dimensional model (Heisenberg chain), this will become:

$$\hat{H}=-\frac{J_{xy}}{2}\cdot\sum_{i}\left[\hat{S}_{i+1}^+\hat{S}_i^-+\hat{S}_i^+\hat{S}_{i+1}^-\right]-J_z\cdot\sum_{i}\hat{S}_{i+1}^z\hat{S}_i^z \tag{3}$$

2.2. The Hubbard model. When the valence electrons of a cristaline lattice are partially itinerant (metals, alloys etc..) the physical properties are studied by considering a many-body hamiltonian in a second quantized form. The most used model in this sens is the Hubbard [13] one. In this model the many-body hamiltonian is obtained by considering Wannier states: $\Phi_{n,\sigma}(\vec{r}-\vec{R}_\alpha)$. This states describe quasi-localized electrons on the n orbital and spin σ, situated at the ion with the $\vec{R}_\alpha$ position.

Presuming that all the itinerant electrons are on the same undegenerated orbital, the Hubbard hamiltonian can be written as:

$$\hat{H}=-\sum_{\alpha,\alpha',\sigma}t_{\alpha,\alpha'}\cdot\hat{a}_{\alpha',\sigma}^+\cdot\hat{a}_{\alpha,\sigma}+U\sum_{\alpha,\sigma}\hat{n}_{\alpha,\sigma}\cdot\hat{n}_{\alpha,-\sigma} \tag{4}$$

We denoted by $\hat{a}_{\alpha,\sigma}^+$ the creation operator of a state with spin σ at the $\vec{R}_\alpha$ lattice point. $\hat{a}_{\alpha,\sigma}$ and $\hat{n}_{\alpha,\sigma}$ are the corresponding annihilation and particle number operators respectively. The first term in (4) is the cinetic energy with $t_{\alpha,\alpha'}$ calculable as:

$$t_{\alpha,\alpha'}=\frac{1}{V}\sum_{K}\varepsilon_K\cdot\exp\left[iK(R_\alpha-R_{\alpha'})\right] \tag{5}$$

The second term in the hamiltonian represents the interaction between the electrons. This interaction is considered strongly screened by the conduction electron gas, and thus approximated in the form of a δ function.

Considering a one dimensional case, and allowing for the valence electrons to jump only at nearest lattice sites, the hamiltonian of the system becomes:

$$\hat{H}=-t\sum_{\alpha,\sigma}(\hat{a}^{+}_{\alpha,\sigma}\hat{a}_{\alpha+1,\sigma}+\hat{a}^{+}_{\alpha+1,\sigma}\hat{a}_{\alpha,\sigma})+U\sum_{\alpha,\sigma}\hat{n}_{\alpha,\sigma}\hat{n}_{\alpha,-\sigma} \tag{6}$$

2.3. Lattice models for itinerant electrons. A more visual way to study interactive electron systems is possible by the second quantification of the many-body hamiltonian in a discretized coordinate space [7,11]. We will illustrate this in a one-dimensional case for quantum particles considered in a $V(x)$ potential.

The time independent Schrödinger equation for a single particle with mass m will be:

$$\hat{H}\psi=-\frac{h^2}{8\pi^2 m}\Delta\psi+V(x)=E\psi \tag{7}$$

Discretizing the problem on a lattice with sites of length a, the differential equation (7) can be written in the form of L ($L\,a=l$ with l the length of the considered space) coupled linear equations

$$\left(-\frac{h^2}{8\pi^2 m a^2}\right)(\psi_{i+1}+\psi_{i-1}-2\psi_i)+V_i\cdot\psi_i=E\psi_i, \tag{8}$$

where ψ_i and V_i denotes the medium values in box i of the lattice for the functions $\psi(x)$ and $V(x)$ respectively. Introducing the notations

$$t=\frac{h^2}{8\pi^2 m a^2} \tag{9}$$

$$W_i=V_i+\frac{h^2}{4\pi^2 m a^2}, \tag{10}$$

equation (8) becomes:

$$-t\cdot(\psi_{i+1}+\psi_{i-1})+W_i\psi_i=E\psi_i \tag{11}$$

We can write now this system of equations in a second quantized form, using as state vectors the n_i occupation number of the cells: $|n_1,n_2,\ldots,n_i,\ldots,n_L\rangle$. Considering the creation, $\hat{c}_i^+$ annihilation $\hat{c}_i$ and the occupation number operators, $\hat{n}_i$, defined by

$$\hat{c}_i^+|n_1,n_2,\ldots,n_i,\ldots,n_L\rangle=\sqrt{n_i+1}\,|n_1,n_2,\ldots,n_i+1,\ldots,n_L\rangle \tag{12}$$

$$\hat{c}_i|n_1,n_2,\ldots,n_i,\ldots,n_L\rangle=\sqrt{n_i}\,|n_1,n_2,\ldots,n_i-1,\ldots,n_L\rangle \tag{13}$$

$$\hat{n}_i|n_1,n_2,\ldots,n_i,\ldots,n_L\rangle=n_i|n_1,n_2,\ldots,n_i,\ldots,n_L\rangle, \tag{14}$$

the wave function of the system becomes

$$\psi=\sum_{i=1}^{L}\psi_i\hat{c}_i^+|0,0,\ldots,0\rangle, \tag{15}$$

and equations (11) can be written as:

$$\sum_{i=1}^{L}\left[-t(\hat{c}_{i+1}^+\psi_i+\hat{c}_i^+\psi_{i+1})+W_i\hat{c}_i^+\psi_i\right]|0,0,\ldots,0\rangle=\sum_{i=1}^{L}E\psi_i\hat{c}_i^+|0,0,\ldots,0\rangle. \tag{16}$$

The second quantized form of the hamiltonian in the considered discretized space will be:

$$\hat{H}=-t\sum_i\left[\hat{c}_i^+\hat{c}_{i+1}+\hat{c}_{i+1}^+\hat{c}_i\right]+\sum_i W_i\hat{n}_i \tag{17}$$

Considering more then one non-interactive particles in the same lattice, the hamiltonian remains unchanged. Interaction between the particles will be introduced via extra terms like:

$$\hat{H}_0=V_0\cdot\sum_i\hat{n}_i(\hat{n}_i-1), \tag{18}$$

or:

$$\hat{H}_1=V_1\cdot\sum_i\hat{n}_i\hat{n}_{i+1} \tag{19}$$

Term (18) represent an on-site repulsion, and (19) the interaction between particles in neighbouring cells. Depending on the sign of V_i this interaction can be attractive or repulsive

Taking into account the spins of the particles, beside the box in which the particle is, we will have an additional discret parameter characterizing the projection of the spin

3. The Quantum Monte Carlo method

We will sketch in the following how the standard Metropolis algorithm can be used for quantum-statistical systems with hamiltonians of the form (3), (6), and (17).

The partition function of a one dimensional system considered on a lattice with L cells, and which is in thermal equilibrium with a heat-bath of temperature T is given by

$$Z=Tr(\exp(-\beta\cdot\hat{H}))=\sum_{\{n_i\}}\langle n_1,n_2,...,n_L|\exp(-\beta\cdot\hat{H})|n_1,n_2,...,n_L\rangle, \tag{20}$$

where the sum is over all the posible combination of the n_i ocupation numbers and $\beta=\frac{1}{k_B\cdot T}$.

A possibility of performing the Monte Carlo simulation would be to diagonalize the hamiltonian, and considering a Metropolis algorithm for the resulted states. If we considar just 2 possible particles in each of the L possible cells, we would have to diagonalize a matrix of $2^L\times 2^L$ which is practically impossible for $L>>1$. If we don't make this diagonalization the calculation of the necessary matrix elements becomes very time-consuming, and a classical Monte Carlo simulation would have the following steps:

- we consider an $\{n_i^0\}$ initial configuration
- we consider a possible $\{n_i^f\}$ new configuration
- we accept the change of configuration $\{n_i^0\}$ in $\{n_i^f\}$ with the probability:

$$P=\frac{\langle\{n_i^f\}|\exp(-\beta\hat{H})|\{n_i^f\}\rangle}{\langle\{n_i^f\}|\exp(-\beta\hat{H})|\{n_i^f\}\rangle+\langle\{n_i^0\}|\exp(-\beta\hat{H})|\{n_i^0\}\rangle} \tag{21}$$

- we continue this algorithm until the thermodinamic equilibrum is reached
- we collect periodically the important and relevant data

The problem with this algorithm is that the calculation of the matrix elements in (21) is very time-consuming, and it is not clear at all which changes will leave to reasonable

transition probabilities.

For a practically succesful realization of the MC simulation we have to rewrite the Z partition function in a form in which the calculation of the P transition probabilities are easy when only a few n_i occupation numbers have been changed. We will sketch how is possible to performe this.

3.1. The Trotter-Suzuki approximation. We will consider the interaction terms of our many-body hamiltonian (17) in the form (18) and (19). This case will include the quantum spins and the Hubbard model too.

Denoting by V_i the interaction terms of the forms $V_0\hat{n}_i(\hat{n}_i-1)$ and $V_1\hat{n}_i\hat{n}_{i+1}$, we separate our hamiltonian in two commuting parts $\hat{H}_a$ and $\hat{H}_b$.

$$\hat{H}_a=(-t\hat{c}_1^+\hat{c}_2-t\hat{c}_2^+\hat{c}_1+\frac{V_1}{2}+\frac{V_2}{2})+(-t\hat{c}_3^+\hat{c}_4-t\hat{c}_4^+\hat{c}_3+\frac{V_3}{2}+\frac{V_4}{2})+\ldots$$
$$\ldots+(-t\hat{c}_{L-1}^+\hat{c}_L-t\hat{c}_L^+\hat{c}_{L-1}+\frac{V_{L-1}}{2}+\frac{V_L}{2})=\hat{H}_1+\hat{H}_3+\ldots+\hat{H}_{L-1}, \tag{22}$$

with:

$$\hat{H}_i=-t\hat{c}_i^+\hat{c}_{i+1}-t\hat{c}_{i+1}^+\hat{c}_i+\frac{V_i}{2}+\frac{V_{i+1}}{2} \tag{23}$$

In a similar way $\hat{H}_b=\hat{H}_2+\hat{H}_4+\ldots+\hat{H}_L$. One can observ immediately that the terms inside $\hat{H}_a$ and $\hat{H}_b$ comute between them, and so:

$$\langle\{n_i\}|\exp(-\beta\hat{H}_a)|\{n_j\}\rangle=\langle\{n_i\}|\exp(-\beta\hat{H}_1)|\{n_j\}\rangle\cdot$$
$$\langle\{n_i\}|\exp(-\beta\hat{H}_3)|\{n_j\}\rangle\cdot\ldots\langle\{n_i\}|\hat{H}_{L-1}|\{n_j\}\rangle \tag{24}$$

The same affirmation is also valid for $\hat{H}_b$.

Ideal it would be to write the partition function as product of exponentials, each of them containing just one $\hat{H}_i$ term. In this way the calculation of the transition probabilities when just a few occupation numbers are changed would be much easier. To achive this we

need to write $\exp\left[-\beta(\hat{H}_a+\hat{H}_b)\right]$ as: $\exp(-\beta\hat{H}_a)\cdot\exp(-\beta\hat{H}_b)$. Unfortunately this equation is not valid anymore, because $\hat{H}_a$ and $\hat{H}_b$ do not commute. However in the case of two $\hat{A}$ and $\hat{B}$ sufficiently small operators one can use the approximation:

$$e^{\hat{A}}\cdot e^{\hat{B}}=e^{\hat{A}+\hat{B}+0,5\cdot[\hat{A},\hat{B}]}\approx e^{\hat{A}+\hat{B}} \tag{25}$$

Considering now M a large integer, so that $\frac{\beta\cdot\hat{H}_a}{M}$ and $\frac{\beta\cdot\hat{H}_b}{M}$ to be small enough, we are able to use the (25) approximation in the form proposed by Trotter and Suzuki [12,14]

$$Z=\sum_{\{n_i\}}\left\langle\{n_i\}\left|\left(\exp\left[-\frac{\beta}{M}\cdot(\hat{H}_a+\hat{H}_b)\right]\right)^M\right|\{n_i\}\right\rangle\approx$$
$$\approx\sum_{\{n_i\}}\left\langle\{n_i\}\left|\left(\exp\left[-\frac{\beta}{M}\cdot\hat{H}_a\right]\cdot\exp\left[-\frac{\beta}{M}\cdot\hat{H}_b\right]\right)^M\right|\{n_i\}\right\rangle \tag{26}$$

To be able of writing Z as a product which in a Monte Carlo simulation can be considered as transition probabilities, we insert between each exponentials in (26) a complet set of states

$$\sum_{\{n_{i,\alpha}\}}\left|n_{1,\alpha},n_{2,\alpha},\ldots,n_{L,\alpha}\right\rangle\left\langle n_{1,\alpha},n_{2,\alpha},\ldots,n_{L,\alpha}\right|.$$

Because each of these $2M$-1 sets represent an independent sum over all the possible states, they will be indexed with a new label, α, which is different from the spatial one, i. The initial trace contribute too to the independent set of states, so the α index can take $2M$ values. Taking account of (22), and remembering that $\hat{H}_i$ acts only on the states n_i and n_{i+1} we can write:

$$Z\sim\sum_{\{n_{i,\alpha}\}}\prod_{\alpha=1}^{2M}\prod_{i=1}^{L}P_{i,\alpha}. \tag{28}$$

For the case when α and i are both even or odd the $P_{i,\alpha}$ factors are calculable as

$$P_{i,\alpha}=\left\langle n_{i,\alpha},n_{i+1,\alpha}\left|e^{-(\Delta\tau\cdot\hat{H}_i)}\right|n_{i,\alpha+1},n_{i+1,\alpha+1}\right\rangle, \tag{29}$$

for all other choices (we used the notation $\Delta\tau=\frac{\beta}{M}$). Because both of the i and α indices label occupation numbers, by using the Trotter-Suzuki (T-S) approximation we created in fact a

two-dimensional lattice from our real one-dimensional one. Every box of the original lattice is multiplied by $2M$ times, and all the $n_{i,\alpha}$ occupation numbers are independent variables. Due to the original trace the α index must satisfy the periodical boundary conditions: $n_{i,2M+1}=n_{i,1}$.

We are able now to consider our quantum-statistical problem as a classical one, characterized by the

$$Z\approx\sum_{\{n_{i,\alpha}\}}\exp(-\beta\sum_{i,\alpha}e_{i,\alpha}) \tag{30}$$

partition function. In equation (30) we used the $-\beta e_{i,\alpha}=\ln P_{i,\alpha}$ notation, every $e_{i,\alpha}$ being calculable from the four $n_{i,\alpha}$, $n_{i+1,\alpha}$, $n_{i,\alpha+1}$ and $n_{i+1,\alpha+1}$ occupation numbers.

We transformed in this way our quantum-statistical problem in a classical one, considered in a space with increased dimensionality. The dimension indexed by i is called spatial, and the one indexed by α is the Trotter or imaginary time direction. It can be shown that the presented method is totally equivalent with the Path Integral [15,16] formulation of the quantum-mechanical problem. (Each two lines in the Trotter direction corresponding to a time intervall of $\Delta\tau$ in the Path Integral formalism.)

4. Performing the Monte Carlo simulation

The Monte Carlo simulation will follow now the known Metropolis algorithm. In the transformed, (30), problem we have four-site interactions between the neighbouring sites $n_{i,\alpha}$, $n_{i+1,\alpha}$, $n_{i,\alpha+1}$ and $n_{i+1,\alpha+1}$, with the values of i and α both even or odd (otherwise $e_{i,\alpha}=0$). In the space of i and α this interaction can be represented by a check-board pattern (Fig. 1), with interactions around the dark plaquets.

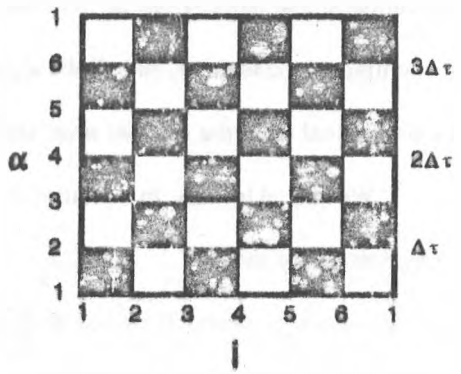

Fig.1 The Caracteristic checkboard pattern considered in the QMC simulations

In many cases the transition probabilty $P'_{i\alpha}$ given by equation (29) can be zero, and so the corresponding state will be realized with zero probability. The condition for $P'_{i\alpha}=0$, is to satisfy around the dark plaquets the condition:

$$n_{i\alpha}+n_{i+1,\alpha}=n_{i,\alpha+1}+n_{i+1,\alpha+1} \tag{31}$$

One will realize immediately that not all the possible changes in the occupation numbers will lead to nonzero transition probabilities, and in fact the changes leading to acceptable configurations are quite limited. To save pretious computer time and calculations, we must know right from the beginning which changes will give nonzero transition probabilities. The acceptable changes considered by us (leading to nonzero transition probabilities) will be:

- the occupation numbers from the left side of a white plaquet are increased by unity, and the values from the right side decreased by unity

- the occupation numbers from the left side of a white plaquet are decreased by unity, and the values from the right site increased by unity

(These changes can be realized only if the occupation numbers will not become negative!)

It is obvious that by satisfying in the beginning the (31) conditions for the whole system, and by considering only the above mentioned changes in the occupation numbers, the algorithm will lead to configurations respecting the (31) conditions. The Metropolis MC algorithm will be now as follows:

- we consider an initial configuration so that condition (31) holds for the whole lattice

- we change the values of the occupation numbers around a white plaquet in the way described earlier

- we calculate the change in the total energy of the system as $\Delta E=\Delta\sum_{i,\alpha} e_{i,\alpha}$, the sum beeing done on the neighbouring dark plaquets

- we accept this change with a probability

$$p=\frac{\exp(-\beta\Delta E)}{\exp(-\beta\Delta E)+1} \tag{32}$$

- we continue the algorithm until thermodynamic equilibrium is reached

- after obtaining the thermodynamical equilibrium we collect periodically the relevant datas

We define one MC step as $2ML$ trials of changing the configuration of the system.

4.1. Calculation of the $e_{i,\alpha}$ factors. Usually the calculation of the $e_{i,\alpha}$ "energies" are not possible analytically, and to obtain them we have to calculate numerically the values of $P_{i,\alpha}$ by expanding in Taylor series the exponential from (29) (this is possible because the series converge rapidly for $p=t.\Delta\tau<<1$)

For the model (1.3) of spinless fermions with interactions between nearest neighbours, we can calculate the $e_{i,\alpha}$ energies analitically, and we obtain

$$e(1,1,1,1)=V_1\cdot\frac{\Delta\tau}{\beta} \tag{33}$$

$$e(0,0,0,0)=0 \tag{34}$$

$$e(0,1,0,1)=e(1,0,1,0)=\frac{\rho}{\beta}-\frac{1}{\beta}\ln\cosh(\rho) \tag{35}$$

$$e(0,1,1,0)=e(1,0,0,1)=\frac{\rho}{\beta}-\frac{1}{\beta}\ln\sinh(\rho) \tag{36}$$

In the above formulas we used the notation $\rho=t.\Delta\tau$.

4.2 Determination of relevant physical quantities. The relevant physical quantities are determined after the thermodynamic equilibrium was reached. The energy and the specific heat can be obtained from the well-known relations:

$$E=-\frac{\partial \ln Z}{\partial\beta} \tag{37}$$

$$C=-\beta^2\cdot\frac{\partial E}{\partial\beta} \tag{38}$$

These equations leads to more complicated formulas than we would expect at the first sight. Performing for example the differentiation in (37) one would get:

$$E=\frac{1}{Z}\sum_{\{n_{i,\alpha}\}}\frac{\partial}{\partial\beta}[\beta\sum_{i,\alpha}e_{i,\alpha}]\cdot\exp(-\beta\sum_{i,\alpha}e_{i,\alpha}) \tag{39}$$

In this way for the average energy we must calculate two averages $<e_{i,\alpha}>$, and $<\beta\frac{\partial e_{i,\alpha}}{\partial\beta}>$. The second term is usually zero in classical systems because the effective hamiltonian is temperature independent, but becomes non-zero in our formalism after the T-S approximation.

As result, the energy of the system will be calculable as:

$$<E>=<e_{i,\alpha}>+<\beta\frac{\partial e_{i,\alpha}}{\partial\beta}> \tag{40}$$

The mathematical formulas for E and C in the case of $S=\frac{1}{2}$ spins are given in [5]. The formulas for the magnetization and susceptibility measured in the z axis directions are the same as the classical ones!

The $2M$ replicas of our real space can be also interpreted as illustrating the quantum evolution

of the many-body system (or quantum fluctuations). In this way beside the possibility of studying the proposed many-body problem we also obtain a visual image inside the specific quantum phenomenas.

4.3. Two and three-dimensional systems. Due to the fact, that the physically interesting problems are mostly the two or three dimensional ones we will sketch shortly the possibilities of studying these systems by QMC methods. The T-S approximation will be applicable in these cases two, and the problem will be transformed again in a classical one with increased dimensionality [17,18].

The main problem in performing QMC simulations for solid-state physics problems is, that for the validity of the T-S approximation we have to increase extraordinally the Trotter dimension (usually M>500), and this complicates technically the simulation. In this way for solid-state physics problems until the present days only one or two-dimensional problems were studied by QMC. The real three-dimensional systems began to be accesible nowadays by the use of performant supercomputers.

For a review article concerning the most important results in QMC we propose [8].

5. The considered simulations

The problem considered by us is the analitically simple case of one quantum particle in an infinite deep potential valley and in statistical equilibrium with a heat-bath of temperature T. As it is well-known, the eigen-values of the energy are given by

$$E_n = \frac{h^2 n^2}{8ml^2}, \tag{41}$$

where l is the thickness of the potential valley, m the mass of the particle and h the Planck

constant. The time-average value of the energy, $< E >_t$, in the canonical ensamble is exactly calculable as:

$$<E>_t = \frac{\sum_n E_n \exp(-\beta E_n)}{\sum_n \exp(-\beta E_n)} \tag{42}$$

We proposed to obtain by QMC simulations the value of $<E>$, and to compare it with the real $<E>_t$ value.

The computer code was elaborated by us in the PASCAL programing language, and it is based on the algorithm presented in section 4. The simulations were performed on a 486 DX IBM-PC (66 MHz) computer.

We considered electrons (m=9,01.10^{-31} kg) and the thickness of the potential valley l=3 $10^{-9}m$. The infinite barriers in our QMC simulations were realized by interdicting for the particle to ocupy the first and the last spatial cells.

Different values for the i number of spacial cells, for the $2M$ Trotter dimension, and for the T temperature of the heat-bath were chosen. In accord with this the p parameters value was also changed, and thus the validity of the Trotter-Suzuki approximation. We proposed to investigate the influence of all these factors on the relative error

$$\varepsilon_R = \frac{|<E> - <E>_t|}{<E>_t}, \tag{43}$$

of the QMC method.

By a very simple argument, based on the fact that the error in Z is mostly due to the considered Trotter-Suzuki approximation, (25), we might expect that in the first approximation ε_R to be of the order:

$$\varepsilon_R \approx \frac{\ln[e^{p+0.5f(p)}] - \ln[e^p]}{\ln[e^p]} \approx \frac{p}{2} \tag{44}$$

We also proposed to verify this hypothesis.

6. Results

Our results are presented on Figs. 2-5. In Fig.2 considering different $i-L$, p and T values we illustrated how the thermodynamic equilibrium is reached during the QMC method

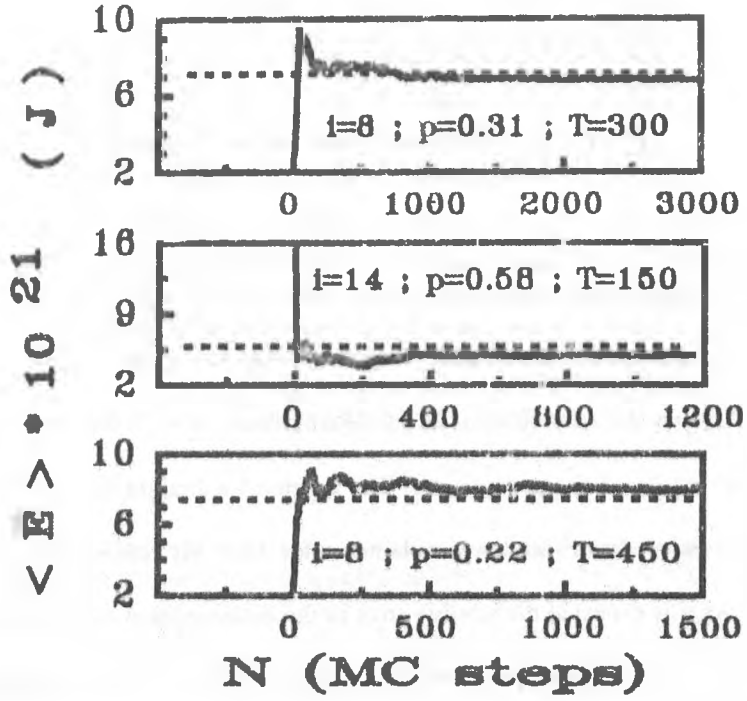

Fig.2 Characteristic variations for the time averaged energy value during simulations.

(As we already mentioned one MC step is considered to be equivalent with $2M\times i$ trials of changing the occupation numbers arround randomly chosen white plaquets.) The dashed straight line is for the theoretical $\langle E \rangle_t$ value. We must mention here, that although the problem is very simple, for realizing 1000 MC steps hours of computer time were necessary (on a PC-type computer). As it is observable from the figures, the inital large fluctuations in

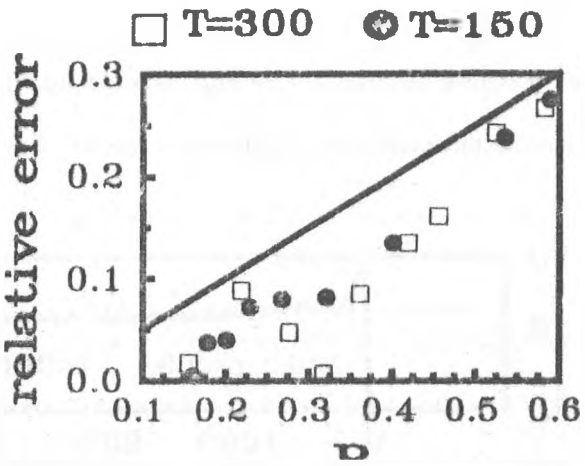

Fig.3 Relative error of our simulation considering two different temperatures and various values for the p parameter. The continuous line represents the $p/2$ argued maximal relative error.

the value of $<E>$ becomes reduced after more than 1000 MC steps.

Fig. 3 shows the relative error in the determination of $<E>$ for T=150 K and T=300 K and various values of the p parameter. The continuous straight line corresponds to the mentioned $p/2$ value. Each result was obtained after 3000 MC steps, and considering i=8 spatial cells. As it is expected the relative error in the determination of the energy is tending to zero as the p parameter becomes smaller and smaller. The $p/2$ value seems to be pretty good estimate for the maximal value of the relative error.

Considering i=8, the same p=0.228 parameter and the same 3000 MC steps, in Fig. 4 we present results concerning the effect of the temperature. It is important for us to be sure that the model works both in the low temperature, quantum-mechanical limit, and in the high temperature, classical limit as well. The results presented here, and the ones from the previous figure suggest that the QMC method works for all the considered temperature, but the relative errors are usually smaller for higher temperatures. The dashed straight line from the figure

illustrate the $p/2$ limit. One can observe that although all the relative errors are smaller than this limit, in reality a dependence from the temperature must also exist.

The influence of the number of considered spatial cells, i, were also investigated.

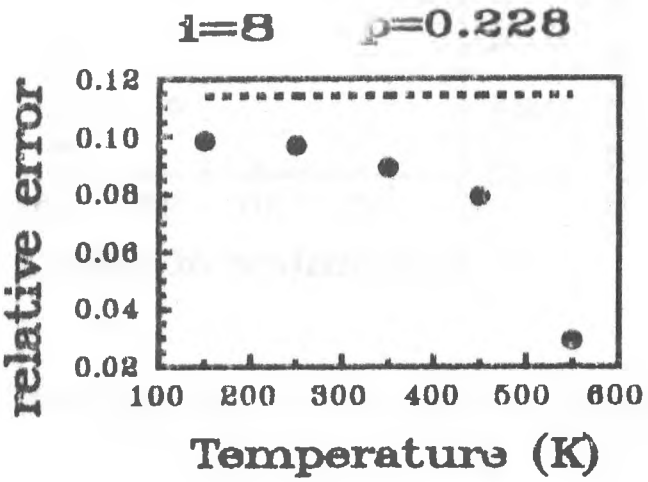

Fig.4 Relative error of the QMC data obtained after 3000 MC steps and different temperatures. The same p and i values are considered and the dashed line coresponds to the $p/2$ limit.

Considering T=150 K, p=0.574 and 3000 MC steps the results in this sense are presented on Fig. 5 (dashed line represents the $p/2$ limit). One would expect that increasing i the error introduced by the space discretization should decrease. This simple argument is proved by our simulations, although the improvements in the result with increasing i are quite small.

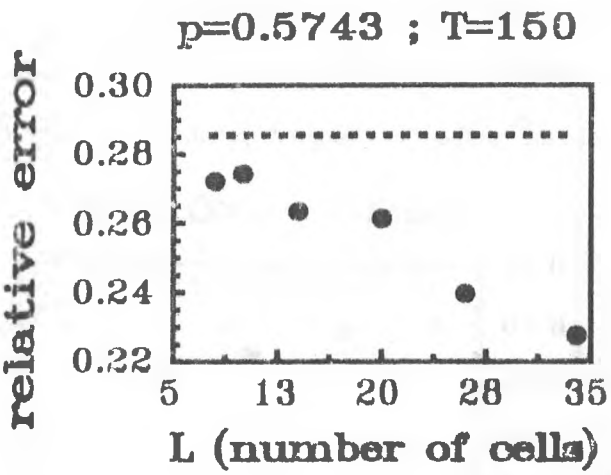

Fig.5 Relative error of the QMC data obtained after 3000 MC steps versus the number L the considered spatial cells. The data points are obtained for the same p parameter and T temperature

7. Conclusions

The results presented in the previous section convince on the applicability of the QMC method. From Figs 2-5 we learn that in the limit $L\to\infty$, $p\to 0$, and for a large number of MC steps the results obtained by the QMC methods are converging to the exact ones. Generally the results obtained for $p\approx 0.2$ are giving a fairly good estimate for the exact one.

The statistical equilibrium values are reached usually considering more than 2000-3000 MC steps. Performing the simulations on PC-type computers and considering large number of spatial cells the applicability of the method becomes technically limited by the necessary computing time, and thus for more complex problems performant workstations are needed.

As a general rule, when the statistical equilibrium is reached we got that $p/2$ is a good estimate for the maximal relative error of the method.

The method works well both in the low and high temperature limits, but for the same value of the p parameter the relative errors are smaller for higher temperatures. As a **general conclusion** we can affirm that the QMC methods offer nice perspectives in studying many-body systems. In the specific problems of condensed matter physics QMC simulations could complete nicely the analitical approximations. Considering interactive electron systems in different potentials, the one- or two-dimensional Hubbard model, or quantum-spin systems many new interesting results were or will be obtained by this method. In the future we plan to contribute in the studies of such theoretically important models.

Acknowledgements

We acknowledge to L. P. Csernai and J. Lovas the pretious discussions we had on the QMC method.

REFERENCES

1 P.W. Anderson; Science **235**, 1196 (1987)
2 S.J. Lee and J.B. Ketterson; Phys. Rev. Lett. **67**, 3078 (1990)
3 H. De Raedt and Ad Lagendijk; Phys. Rep. **127**, 233 (1985)
4 V.V. Ulyanov and O.B. Zaslavskii; Phys. Rep. **216**, 181 (1992)
5 J.C. Cullen and D.P. Landau; Phys. Rev. B **27**, 297 (1983)
6 M. Creutz; Quarks, Gluons and Lattices, (Cambridge Univ. Press, 1983)
7 J. Tobochnik, G. Batrouni and H. Gould, Computers in Physics 6, 673 (1992)
8 W. von der Linden; Phys. Rep. **220**, 53 (1992) and Int. J. Mod. Phys. C **4**, 341 (1993)
9 M.C. Bohm, J. Schulte, L. Utrera; Mol. Phys. **79**, 1239 (1993)
10 Quantum Monte Carlo Methods; ed. M. Suzuki (Springer-Verlag, New-York, 1987)
11 G.G. Batrouni, R.T. Scalettar and G.T. Zimanyi; Phys. Rev. Lett. **65**, 1765 (1990) and **66**, 3144 (1991)
12 M. Suzuki, Prog. Theor. Phys. **56**, 1454 (1976)
13 J. Hubbard, Proc. R. Soc. London A **276**, 238 (1963)

14. H.F. Trotter; Proc. Am. Math. Soc. **10**, 545 (1959)
15. J. Tobochnic, H. Gould and K. Mulder; Comput. Phys. **4**,431 (1990)
16. W. Krauth, N. Trivedi and C. Ceperly; Phys. Rev. Lett. **67**, 2307 (1991)
17. M.S. Makivic H.-Q. Ding; Phys. Rev. B **43**, 3562 (1991)
18. T. Onogi, S. Miyashita and M. Suzuki; in Quantum Monte Carlo Methods, ed. M. Suzuki (Springer-Verlag, New-York, 1987)

In cel de al XXXIX-lea an (1994) *Studia Universitatis Babeş-Bolyai* apare în următoarele serii:

matematică (trimestrial)
fizică (semestrial)
chimie (semestrial)
geologie (semestrial)
geografie (semestrial)
biologie (semestrial)
filozofie (semestrial)
sociologie-politologie (semestrial)
psihologie-pedagogie (semestrial)
ştiinţe economice (semestrial)
ştiinţe juridice (semestrial)
istorie (semestrial)
filologie (trimestrial)
teologie ortodoxă (semestrial)

In the XXXIX-th year of its publication (1994) *Studia Universitatis Babeş-Bolyai* is issued in the following series:

mathematics (quarterly)
physics (semesterily)
chemistry (semesterily)
geology (semesterily)
geography (semesterily)
biology (semesterily)
philosophy (semesterily)
sociology-politology (semesterily)
psychology-pedagogy (semesterily)
economic sciences (semesterily)
juridical sciences (semesterily)
history (semesterily)
philology (quarterly)
ortodox theology (semesterily)

Dans sa XXXIX-e année (1994) *Studia Universitatis Babeş-Bolyai* paraît dans les séries suivantes:

mathématiques (trimestriellement)
physique (semestriellement)
chimie (semestriellement)
geologie (semestriellement)
géographie (semestriellement)
biologie (semestriellement)
philosophie (semestriellement)
sociologie-politologie (semestriellement)
psyhologie-pédagogie (semestriellement)
sciences économiques (semestriellement)
sciences juridiques (semestriellement)
histoire (semestriellement)
philologie (trimestriellement)
théologie ortodoxe (semestriellement)